$CD20^+$ T follicular helper-like cells drive antigen-specific autoimmunity in bullous pemphigoid

Authors:

Hui Fang[1,†], Shengxian Shen[1,†], Kang Li[1,†], Tianyu Cao[2,†], Bing Wang[1], Haijun Miao[1], Ke Xue[1], Yaxing Bai[1], Liang Li[1], Xia Li[1], Pei Qiao[1], Jieyu Zhang[1], Huanhuan Qu[1], Chen Zhang[1], Chunying Xiao[1], Bingyu Pang[1], Meng Fu[1], Hongjiang Qiao[1], Shuai Shao[1,*], Erle Dang[1,*], Gang Wang[1,*]

Affiliations:

[1]Department of Dermatology, Xijing Hospital, Fourth Military Medical University; Xi'an, Shaanxi, 710032, China.

[2]Department of Dermatology, Tangdu Hospital, Fourth Military Medical University, Xi'an, Shaanxi, 710032, China.

[†]These authors contributed equally to this study.

***Corresponding author:**

Gang Wang, MD, PhD, Department of Dermatology, Xijing Hospital, Fourth Military Medical University, 127 Changlexi Road, Xi'an 710032, China. E-mail: xjwgang@fmmu.edu.cn. Tel: 86-29-84771244

Erle Dang, PhD, Department of Dermatology, Xijing Hospital, Fourth Military Medical University, 127 Changlexi Road, Xi'an 710032, China. E-mail: dangerle@fmmu.edu.cn. Tel: 86-29-84771244

Shuai Shao, MD, PhD, Department of Dermatology, Xijing Hospital, Fourth Military Medical University, 127 Changlexi Road, Xi'an 710032, China. E-mail: shaos@fmmu.edu.cn. Tel: 86-29-84771244

Conflict of interest statement: The authors have declared that no conflict of interest exists.

Abstract

$CD20^+$ T cells are increasingly recognized as drivers of autoimmune and inflammatory diseases. However, their origin, development, and specific role in autoimmune skin diseases remain poorly understood. In this study, we observed an expansion of $CD20^+$ T cells in the peripheral blood and skin lesions of patients with bullous pemphigoid (BP), which correlated with the levels of pathogenic autoantibodies and disease severity. Compared with $CD20^-$ T cells, $CD20^+$ T cells exhibited enhanced metabolic and proinflammatory activities. In particular, antigen-specific BP180-NC16A-reactive T cells were enriched within the $CD4^+CD20^+$ subset. In both patients with BP and BP180-immunized mice, $CD4^+CD20^+$ T cells exhibited an antigen-specific follicular helper T (Tfh)-like phenotype, facilitating antibody production and B cell differentiation, whereas $CD8^+CD20^+$ T cells displayed cytotoxic and proinflammatory features. Mechanistically, we found that expression of the CD20-encoding gene *MS4A1* in T cells was regulated by PAX5 in a DNA methylation-dependent manner. Therefore, our study elucidates the regulatory mechanisms governing $CD20^+$ T cells and highlights their important role in the pathogenesis of BP.

Keywords: $CD20^+$ T cells, autoimmune diseases, B cell, autoantibody production, PAX5

INTRODUCTION

CD20 is a surface molecule classically expressed on B lymphocytes from early developmental stages through maturity, but it is absent on terminally differentiated plasmablasts and plasma cells (1). Over two decades ago, a subset of human $CD3^+$ T cells in the peripheral blood was shown to express CD20, albeit at low levels compared with those of B cells (2). Recent research has increasingly highlighted the role of these $CD20^+$ T cells in various autoimmune diseases, such as multiple sclerosis (3-5), rheumatoid arthritis (6, 7), primary Sjögren's syndrome (8), and psoriasis (9), as well as obesity (10) and cancer (11). Notably, therapies targeting CD20, such as rituximab (RTX), deplete both $CD20^+$ B cells and $CD20^+$ T cells, effectively reducing inflammation in patients with diseases such as multiple sclerosis (12). Despite these findings, the origins and functions of $CD20^+$ T cells in autoimmune skin diseases remain incompletely understood.

Autoimmune diseases are characterized by aberrant interactions between T cells and B cells, leading to the production of autoantibodies. T cells play pivotal roles in autoimmune pathogenesis by promoting B cell survival, differentiation, antibody production, as well as by secreting proinflammatory cytokines (13, 14). Bullous pemphigoid (BP), a common autoimmune blistering skin disorder, is characterized by autoantibodies targeting proteins at the dermal–epidermal junction (BP180 and BP230), which clinically manifests as tense blisters and erosions on the skin surface (15). Our previous study identified two major T cell epitope peptides, P2 (492-506 aa: VRKLKARVDELERIR) and P5 (501-515 aa: ELERIRRSILPYGDS), highlighting their substantial roles in stimulating $CD4^+$ T cell proliferation, interleukin (IL)-4 production, and the activation of autoantibody-secreting B cells (16). Additionally, multiple T cell abnormalities have been documented in BP, including expansion of activated T helper 2 (Th2) cells (17), Th17 cells (18) and follicular helper T (Tfh) cells (19), as well as dysfunction of regulatory T cells (20, 21).

However, the specific contributions of $CD20^+$ T cells to the pathogenesis of BP remain unclear.

In the present study, we investigated $CD20^+$ T cells in peripheral blood and skin lesions from patients with BP, as well as in BP180-immunized mice. We found that $CD20^+$ T cells were markedly expanded in both the circulation and lesional skin of patients with BP, and that this expansion correlated with disease severity. Compared with $CD20^-$ T cells, $CD20^+$ T cells displayed enhanced proliferative capacity, autoreactivity to BP autoantigens, and increased metabolic activity. In both patients with BP and BP180-immunized mice, $CD4^+CD20^+$ T cells exhibited an antigen-specific Tfh-like phenotype, characterized by heightened responsiveness to BP autoantigens, increased IL-21 production, and a greater capacity to promote B cell differentiation and autoantibody generation, whereas $CD8^+CD20^+$ T cells displayed predominantly cytotoxic and proinflammatory features. Mechanistically, we further demonstrated that *MS4A1*, the gene encoding CD20, is endogenously expressed in human T cells and is regulated by DNA methylation and the transcription factor PAX5. Together, these findings identify functionally distinct $CD20^+$ T cell subsets in BP and provide insight into the regulatory mechanisms underlying CD20 expression and pathogenic T cell function.

RESULTS

$CD20^+$ T cells expand in the peripheral blood and skin lesions of BP patients

To explore the potential involvement of $CD3^+CD20^+$ T cells in BP pathogenesis, we compared their levels in BP patients and sex- and age-matched healthy controls via flow cytometry. Our analyses revealed significantly higher percentages of $CD3^+CD20^+$ T cells in the peripheral blood of BP patients than in that of healthy controls (Figure 1, A and B). Additionally, the frequencies of these $CD20^+$ T cells were significantly positively correlated with the serum titer of anti-BP180

NC16A IgG, a key biomarker of disease severity (Figure 1C). Previous studies have shown that $CD20^+$ T cells encompass both $CD4^+$ and $CD8^+$ subpopulations (3). Our analysis of gated $CD3^+CD20^+$ T cells in the circulation revealed an increase in the $CD4^+CD20^+$ T cell subpopulation in BP patients compared with healthy controls, although the difference was not statistically significant (Supplemental Figure 1, A and B). After corticosteroid treatment, which is typically the initial therapy for BP, there was no significant change in the overall frequency of $CD3^+CD20^+$ T cells (Supplemental Figure 1, C and D). However, we observed a shift in the $CD4^+$ and $CD8^+$ subpopulations within $CD20^+$ T cells after corticosteroid treatment: the proportion of $CD4^+CD20^+$ T cells decreased, whereas that of $CD8^+CD20^+$ T cells increased (Figure 1D and Supplemental Figure 1, D and E).

To further investigate the circulating immunological changes in BP, we performed single-cell RNA sequencing (scRNA-seq) on immune cells isolated from 3 patients with active BP and 3 age- and sex-matched healthy controls (Supplemental Figure 2, A and B). Following quality control, a total of 52,794 high-quality cells (25,073 from healthy controls and 27,721 from BP patients) were used for further analysis. Using a standard single-cell analysis pipeline, we identified 15 distinct clusters (Supplemental Figure 2C). On the basis of canonical marker gene expression, these clusters were classified into seven major immune cell types: T cells, B cells, natural killer (NK) cells, monocytes, granulocytes, megakaryocytes and dendritic cells (Supplemental Figure 2, D and E). Comparative analysis revealed marked shifts in immune cell proportions, including reduced levels of T cells and NK cells and increased proportions of monocytes and granulocytes, in BP patients compared with healthy controls (Supplemental Figure 2F). Consistent with the flow cytometry data, our scRNA-seq analysis revealed a T cell subset expressing the classical B cell marker gene *MS4A1* in both BP patients and healthy controls (Figure 1E). Cluster proportion

analysis revealed that an increased proportion of $CD3^+CD20^+$ T cells was accompanied by a corresponding decrease in $CD3^+CD20^-$ T cells in BP patients (Figure 1F). Quantification revealed that $CD8^+CD20^+$ T cells constituted a substantial proportion of T cells in both groups. Strikingly, the proportion of $CD4^+CD20^+$ T cells was significantly greater in the BP group than in the healthy control group (Figure 1G).

Next, we investigated whether $CD20^+$ T cells were also present in the inflamed skin tissues of BP patients and other skin diseases. Confocal imaging revealed the colocalization of CD20 with the classic T cell marker CD3 and the B cell marker CD19, confirming the presence of both $CD3^+CD20^+$ T cells and $CD19^+CD20^+$ B cells in BP skin lesions (Figure 1H). Interestingly, we also detected the presence of $CD3^+CD20^+$ T cells in blister fluid (BF), a body fluid that is specifically enriched with innate and adaptive immune cells in BP (Supplemental Figure 3, A and B). Notably, $CD3^+CD20^+$ T cells were absent in lesions from patients with other autoimmune and inflammatory skin conditions, such as pemphigus vulgaris, psoriasis, and lichen planus (Supplemental Figure 3B). Among the $CD3^+$ T cells infiltrating BP lesions, $CD3^+CD20^+$ T cells were more prevalent than $CD3^+CD20^-$ T cells (Figure 1I and Supplemental Figure 4, A and B). Furthermore, the abundance of $CD3^+CD20^+$ T cells in skin lesions was positively correlated with the titers of anti-BP180 NC16A antibodies (Figure 1J). Immunofluorescence analysis further demonstrated that $CD4^+CD20^+$ T cells, not $CD8^+CD20^+$ T cells, constituted the major infiltrating $CD20^+$ T cell subpopulation in BP skin lesions (Figure 1K). Collectively, these results demonstrate that the expansion of $CD20^+$ T cells in the peripheral blood and skin lesions of BP patients is correlated with disease severity.

CD20$^+$ T cells are the predominant BP180-NC16A antigen-specific T cells with enhanced metabolic and proinflammatory activities in BP

To gain deeper insights into the functions and transcriptional profile of CD20$^+$ T cells, we sorted and performed RNA sequencing (RNA-seq) analysis on CD3$^+$CD20$^+$ T cells, CD3$^+$CD20$^-$ T cells, and CD19$^+$ B cells from BP patients and sex- and age-matched healthy controls (n = 3 per group; sorting strategy shown in Supplemental Figure 5A). Our analysis revealed a total of 2,062 and 2,485 differentially expressed genes (DEGs) (FC $\geqslant 1.5$, $P < 0.05$) between CD19$^+$ B cells and CD3$^+$CD20$^+$ T cells from BP patients and healthy controls, respectively (Supplemental Figure 5B). Notably, CD3$^+$CD20$^+$ T cells presented upregulated expression of surface markers such as *CD3, CD4, CD5, CD8* and *CD28* but downregulated expression of *CD40, CD74, CD79A* and *CD79B.* Importantly, compared with CD19$^+$ B cells, CD20$^+$ T cells did not express *CD19, CD86, or CD22* , suggesting their lineage-specific differences from B cells (Supplemental Figure 5C).

By comparing CD3$^+$CD20$^+$ T cells and CD3$^+$CD20$^-$ T cells between BP patients and healthy controls, we identified 752 upregulated and 305 downregulated genes between CD3$^+$CD20$^+$ T cells and CD3$^+$CD20$^-$ T cells from BP patients. In healthy controls, compared with CD3$^+$CD20$^-$ T cells, CD3$^+$CD20$^+$ T cells presented 357 upregulated genes and 275 downregulated genes (Figure 2A). In BP patients, CD3$^+$CD20$^+$ T cells presented elevated expression levels of genes associated with various biological functions, including cell proliferation (e.g., *MKI67*), cytokine and chemokine production (e.g., *IL15, CXCL8, CCL3*), granular protease activity (e.g., *GZMK*), metabolic processes (e.g., *ALG9, GCNT1, ADPRH*), epigenetic modifications (e.g., *LCMT1*), transporters (e.g., *SLC39A7*), and voltage-gated calcium channels (e.g., *CACNA1D*), compared with CD3$^+$CD20$^-$ T cells (Figure 2B). Gene ontology (GO) analysis further demonstrated enrichment of pathways related to S-adenosyl-L-methionine binding, cytokine production involved in the

immune response, glycolipid metabolic processes and cellular calcium ion homeostasis in $CD20^+$ T cells from both BP patients and healthy controls (Figure 2C). Consistent with these findings, gene set enrichment analysis (GSEA) showed statistically significant enrichment of genes associated with the inflammatory response and calcium-mediated signaling in $CD20^+$ T cells compared with those in $CD20^-$ T cells (Figure 2D). Among all the upregulated genes, Kyoto Encyclopedia of Genes and Genomes (KEGG) analysis revealed enrichment of metabolic pathways, such as glyoxylate and dicarboxylate metabolism, carbon metabolism, pyruvate metabolism and cholesterol metabolism, specifically in BP $CD20^+$ T cells, underscoring their heightened metabolic activity under disease conditions (Figure 2E).

To assess the functional responsiveness of $CD20^+$ T cells to BP autoantigens, we compared the proliferative and cytokine responses of $CD20^+$ and $CD20^-$ T cell subsets following stimulation with BP180-NC16A peptides. We found that compared with $CD20^-$ T cells, $CD20^+$ T cells displayed increased proliferative capacity when stimulated with peptides in vitro (Figure 3A and Supplemental Figure 6A). Previous research has highlighted the proinflammatory role of $CD20^+$ T cells, which produce cytokines such as interferon (IFN)-γ and tumor necrosis factor (TNF)-α in diverse autoimmune contexts (4, 22). Notably, intracellular staining showed that the $CD20^+$ T cells produced significant amounts of IFN-γ, IL-4, and IL-17 with or without peptide stimulation when compared with $CD20^-$ T cells, suggesting the enhanced proinflammatory abilities of $CD20^+$ T cells in BP (Figure 3B and Supplemental Figure 6B). We also found that stimulation of T cells with anti-CD3/CD28 Dynabeads for 72 hours increased CD20 expression, suggesting that TCR activation promotes CD20 upregulation in T cells (Supplemental Figure 7, A-D).

Our previous research identified key HLA-DR-restricted T cell epitopes within BP180-NC16A, such as P5 (501-515 aa: ELERIRRSILPYGDS), which play pivotal roles in BP

pathogenesis (16). To further assess the antigen specificity of $CD20^+$ T cells in BP, we developed a peptide-MHC II (pMHC II) tetramer to detect these cells ex vivo in the peripheral blood of untreated BP patients and HLA allele-matched healthy controls. Flow cytometry analysis revealed a greater proportion of tetramer-positive $CD4^+$ T cells in BP patients than in healthy controls under resting conditions (Figure 3C and Supplemental Figure 8A), suggesting prior antigen exposure in BP patients. Upon stimulation with pooled peptides, the frequency of tetramer-positive $CD4^+$ T cells increased further compared with non-stimulated PBMCs from the same patients (Figure 3C and Supplemental Figure 8A). Notably, when comparing tetramer-positive cells within the $CD4^+CD20^+$ and $CD4^+CD20^-$ subsets, we found a markedly higher frequency of tetramer-positive $CD4^+CD20^+$ T cells in BP patients than in healthy controls, both with and without peptide stimulation (Figure 3D and Supplemental Figure 8B), indicating a greater proportion of antigen-specific T cells among the $CD20^+$ T cells. These findings demonstrate that in BP, antigen-specific T cells are enriched within $CD20^+$ T cells, which exhibit heightened responsiveness to autoantigens and enhanced proliferation and elevated metabolic activity.

$CD4^+CD20^+$ T cells exhibit characteristics of Tfh-like cells and produce high levels of IL-21 in BP

To further investigate the functional polarization of $CD3^+CD20^+$ T cells in BP, we performed GSEA pathway analysis on this subset. Our bulk RNA-seq data revealed significant enrichment of genes associated with Tfh cell differentiation in $CD3^+CD20^+$ cells compared with $CD3^+CD20^-$ T cells in BP (Figure 4A). Given that Tfh cells are primarily a $CD4^+$ T cell subset, we next performed more detailed analyses of $CD4^+CD20^+$ and $CD8^+CD20^+$ T cells. Single-cell RNA-seq analysis showed that $CD4^+CD20^+$ T cells exhibited higher expression of membrane molecules (e.g.,

PDCD1, CD40LG, CD69, TNFRSF4), receptors (*CCR4, CXCR3*), effector molecules (*IL4, CCL4, GZMK*), and transcription factors (*MAF, BCL6* and *GATA3*) than $CD4^+CD20^-$ T cells. Compared with $CD8^+CD20^-$ T cells, $CD8^+CD20^+$ T cells displayed higher expression of T cell activation and costimulatory molecules (*CD69, TNFRSF9, CD27, PDCD1, ICOS*) , as well as *GZMK* (Figure 4B). Consistent with these transcriptional profiles, GO analysis revealed that $CD4^+CD20^+$ T cells were enriched in biological processes including B cell activation, T cell migration, T cell differentiation, and regulation of T cell activation, whereas $CD8^+CD20^+$ T cells were enriched in functions related to defense response to virus and T cell-mediated cytotoxicity (Figure 4C). GSEA further demonstrated significant enrichment of mature B cell differentiation and positive regulation of T cell activation in $CD4^+CD20^+$ T cells, whereas T cell-mediated cytotoxicity and inflammatory cytokine production were preferentially enriched in $CD8^+CD20^+$ T cells (Figure 4D and Supplemental Figure 9).

Next, we examined the secretion of cytokines and proteases by $CD4^+CD20^+$ T cells and $CD8^+CD20^+$ T cells in healthy controls and BP patients. Flow cytometry analysis revealed that in both healthy controls and BP patients, $CD4^+CD20^+$ T cells produced higher levels of IL-4, IL-17, and IL-21 compared to $CD8^+CD20^+$ T cells. Conversely, $CD8^+CD20^+$ T cells from both groups secreted greater amounts of IFN-γ, granzyme B, and perforin than $CD4^+CD20^+$ T cells (Supplemental Figure 10A-L). These data suggest that in BP, $CD4^+CD20^+$ T cells are functionally skewed toward B cell help functions and immune activation, whereas $CD8^+CD20^+$ T cells display a more cytotoxic and proinflammatory profile.

To explore whether $CD4^+CD20^+$ T cells exhibit Tfh-like features, we further assessed the expression of CXCR5 and PD-1, two canonical markers associated with Tfh cells. Flow cytometry analysis revealed a greater proportion of $CXCR5^+PD\text{-}1^+$ cells among $CD4^+CD20^+$ T cells than

among $CD4^+CD20^-$ T cells (Figure 4E and Supplemental Figure 11, A and B). Notably, IL-21, a key effector cytokine involved in Tfh-mediated B cell help (23), was expressed at higher levels in $CD4^+CD20^+$ T cells from BP patients than in $CD4^+CD20^-$ T cells (Figure 4F and Supplemental Figure 11C). Consistent with this phenotype, BCL6 and MAF, two transcription factors associated with Tfh-like differentiation, showed higher expression in $CD4^+CD20^+$ T cells than in $CD4^+CD20^-$ T cells in both BP patients and healthy controls (Supplemental Figure 11D-G). Finally, immunofluorescence analysis demonstrated colocalization of CD4, CD20, and CXCR5 in BP skin lesions (Supplemental Figure 12), providing in situ evidence that these cells exhibit Tfh-like features within the lesional microenvironment. Together, these data indicate that $CD4^+CD20^+$ T cells in BP display a pronounced Tfh-like phenotype characterized by expression of CXCR5, PD-1, BCL6, MAF, and IL-21, supporting their potential role in promoting B cell activation and autoantibody production.

$CD4^+CD20^+$ T cells are involved in B cell differentiation and autoantibody production

To further investigate the role of $CD20^+$ T cells in the development of key features associated with BP, we established an active immunization model by immunizing SJL/J mice with a recombinant fragment of murine BP180 (24). Following immunization, all SJL/J mice developed BP180-specific IgG antibodies, which peaked at 4 weeks postimmunization (Figure 5A). Immunofluorescence microscopy confirmed the binding of circulating IgG and complement component C3 to the basement membrane zone, indication successful induction of BP-specific humoral autoimmunity in this model (Figure 5B). Flow cytometry analysis showed that the frequency of $CD3^+CD20^+$ T cells was increased in the spleen, lymph nodes, and peripheral blood of BP180-immunized mice compared with control mice (Supplemental Figure 13, A and B).

Among total $CD3^+$ T cells, the frequency of $CD4^+CD20^+$ T cells was increased in the spleen and peripheral blood of BP180-immunized mice, whereas the frequency of $CD8^+CD20^+$ T cells was not significantly different between the two groups (Figure 5C and Supplemental Figure 13C-E). Furthermore, analysis of the proportions of $CD4^+$ and $CD8^+$ T cells within the $CD3^+CD20^+$ T cell population revealed that the proportion of $CD4^+CD20^+$ T cells was significantly higher than that of $CD8^+CD20^+$ T cells in both control and BP180-immunized mice (Supplemental Figure 14, A and B).

We next examined whether murine $CD4^+CD20^+$ T cells displayed Tfh-like features similar to those observed in human BP. Compared with $CD4^+CD20^-$ T cells, $CD4^+CD20^+$ T cells from BP180-immunized mice contained a higher proportion of $CXCR5^+PD\text{-}1^+$ T cells (Figure 5D and Supplemental Figure 15A). $CD4^+CD20^+$ T cells also produced more IL-21 and expressed higher levels of the transcription factors BCL6 and MAF than $CD4^+CD20^-$ T cells in both control and BP180-immunized mice (Figure 5E and Supplemental Figure 15, B-F). These findings indicate that $CD4^+CD20^+$ T cells in the BP180-immunized mouse model exhibit Tfh-like phenotype resembling that observed in patients with BP.

To further assess the cellular interactions of $CD20^+$ T cells, we analyzed cell-cell communication networks reconstructed from the scRNA-seq dataset. Interactions of $CD20^+$ T cells with dendritic cells, monocytes, NK cells, and B cells were markedly enriched relative to those of $CD20^-$ T cells, suggesting that $CD20^+$ T cells are integrated into an immune network that may amplify pathological responses (Supplemental Figure 16). We next directly tested the B cell helper capacity of distinct T cell subsets. The indicated T cell subsets ($CD4^+CD20^+$, $CD4^+CD20^-$, and $CD8^+CD20^+$ T cells) and $B220^+$ B cells were sorted from the spleens and inguinal lymph nodes of BP180- immunized mice and subjected to ex vivo coculture assays. Compared with $CD4^+CD20^-$ T

cells and $CD8^+CD20^+$ T cells, $CD4^+CD20^+$ T cells more efficiently promoted B cell differentiation into IgD^-CD138^+ plasma cells and $GL7^+Fas^+$ germinal center (GC) B cells, as well as enhanced autoantibody production (Figure 5F and Supplemental Figure 17, A-D).

To determine whether these functional differences were also evident in vivo, we performed adoptive transfer experiments in $Rag1^{-/-}$ mice, which lack mature lymphocytes (Supplemental Figure 18A). ELISA of serum from recipient mice revealed higher levels of anti-BP180 antibodies in those that received $CD4^+CD20^+$ T cells and B cells than in those that received other T cell subsets with B cells or B cells alone (Figure 5G). Consistent with these serological findings, analysis of splenocytes revealed increased frequencies of $GL7^+Fas^+$ GC B cells and IgD^-CD138^+ plasma cells in mice receiving $CD4^+CD20^+$ T cells plus B cells compared with the other recipient groups (Figure 5H and Supplemental Figure 18, B and C). Importantly, treatment with an IL-21-neutralizing antibody significantly attenuated the capacity of $CD4^+CD20^+$ T cells to promote B cell differentiation and antibody production (Figure 5, G and H and Supplemental Figure 18, B and C), indicating that the pathogenic B cell helper activity of this subset depends, at least in part, on IL-21-mediated Tfh-like effector function. Under these transfer conditions, recipient $Rag1^{-/-}$ mice did not develop overt BP-like blistering, indicating that this system models pathogenic B cell help rather than complete disease recapitulation.

Finally, to explore the functional role of CD20 expression, we isolated primary mouse T cells and generated *MS4A1*-knockout (KO) T cells by lentiviral transduction. The proportions of $CD3^+CD20^+$ and $CD4^+CD20^+$ T cells were reduced in *MS4A1*-KO T cells (Supplemental Figure 19, A-D). In addition, compared with negative control (NC)-KO T cells, *MS4A1*-KO T cells showed reduced proportions of $CD4^+CXCR5^+PD\text{-}1^+$ Tfh cells and decreased intracellular IL-21 production (Figure 5, I and J, and Supplemental Figure 19, E and F). These findings demonstrate

that $CD4^+CD20^+$ T cells are expanded in BP180-immunized mice, exhibit Tfh-like characteristics, and actively promote B cell differentiation and pathogenic antibody production.

Endogenous CD20 expression in human $CD20^+$ T cells is regulated by the transcription factor PAX5

The origin of $CD3^+CD20^+$ T cells remains controversial. Some studies have reported that these cells endogenously express CD20 mRNA (*MS4A1*) (25, 26), whereas others have suggested that CD20 may be acquired from B cells through trogocytosis (4). To address this question, we first examined *MS4A1* expression in our bulk RNA-seq dataset. As expected, $CD19^+$ B cells showed high levels of *MS4A1* expression, whereas $CD20^+$ T cells expressed low but detectable levels of *MS4A1*, and $CD20^-$ T cells showed little to no expression in both healthy controls and BP patients (Figure 6A). To further determine whether T cells independently express CD20, we isolated $CD20^+$ T cells, $CD20^-$ T cells, and B cells from healthy donors via fluorescence-activated cell sorting. Quantitative real-time PCR analysis with three different *MS4A1* primer pairs confirmed that $CD20^+$ T cells exhibited endogenous expression of *MS4A1*, albeit at lower levels than in B cells (Figure 6, B and C). Furthermore, fluorescence in situ hybridization revealed CD20 signals in a portion of $CD3^+$ T cells from the BP skin lesions (Figure 6D). These results indicate that $CD20^+$ T cells endogenously express CD20.

To identify regulators of CD20 expression in T cells, we next analyzed transcription factors differentially expressed between $CD20^+$ T cells and $CD20^-$ T cells in the bulk RNA-seq dataset. Among the transcription factors enriched in $CD20^+$ T cells, we identified several lineage-associated regulators, including *PAX5*, *TCF3*, and *ZBTB7B* (Figure 7A). We subsequently screened for transcription factors with potential binding affinity for the *MS4A1* promoter region.

Using de novo sequence motif searches of sequences within the *MS4A1* promoter region, we identified motifs resembling the consensus binding sequences for the transcription factor PAX5 (Figure 7B). To confirm the role of PAX5 in regulating *MS4A1* expression through its promoter, we conducted a luciferase reporter assay in HEK293T cells. Compared with the wild-type promoter, mutation of the PAX5-binding site significantly reduced luciferase activity, confirming the role of PAX5 in activating *MS4A1* expression (Figure 7C). RNA-seq analysis revealed a slight increase in *PAX5* mRNA levels in $CD20^+$ T cells compared with $CD20^-$ T cells from BP patients (Figure 7D). Immunofluorescence analysis revealed that peripheral blood B cells strongly expressed both CD20 and PAX5 whereas $CD20^+$ T cells presented lower expression of both proteins, and $CD20^-$ T cells did not express PAX5 (Figure 7E). We next asked whether T cell activation could induce the PAX5-CD20 axis. Primary human T cells were isolated and stimulated with anti-CD3/CD28 Dynabeads, and PAX5 expression was monitored over time. Upon stimulation, PAX5 expression increased in a time-dependent manner and peaked at 72 hours post-stimulation (Supplemental Figure 20, A and B), consistent with activation-induced engagement of this pathway in T cells.

Although PAX5 is well known for its role in B cell development (27, 28), its association with MS4A1 regulation in T cells has not been previously described. To more directly test the role of PAX5 in regulating CD20 expression in T cells, we generated *PAX5*-knockout primary human T cells using CRISPR-Cas9 technology and confirmed efficient knockout by RT-qPCR after lentiviral transduction (Supplemental Figure 21A). Loss of *PAX5* resulted in a marked reduction in *MS4A1* mRNA levels, accompanied by decreased frequencies of total $CD20^+$ T cells as well as $CD4^+CD20^+$ and $CD8^+CD20^+$ T cell subsets (Figure 7, F and G, and Supplemental Figure 21, B-E), supporting an important role for PAX5 in maintaining CD20 expression in T cells. In addition,

PAX5 deficiency was associated with reduced frequencies of $CD4^+CXCR5^+PD\text{-}1^+$ T cells and decreased IL-21 and IFN-γ production relative to NC-KO T cells (Figure 7, H and I, and Supplemental Figure 21, G-J), suggesting that PAX5 also contributes to the maintenance of Tfh-like features in this context. Together, these data support a model in which PAX5 contributes to endogenous CD20 expression in T cells and helps sustain aspects of the Tfh-like program associated with $CD20^+$ T cells.

The differentiation of $CD20^+$ T cells is regulated by DNA methylation

We next examined the impact of PAX5 overexpression on T cell differentiation. Notably, overexpressing *PAX5* via lentiviral transduction did not significantly increase *MS4A1* mRNA levels (Figure 8A), although the expression levels of *PAX5* were 5–10 times higher than those in control cells (Supplemental Figure 22A). Similarly, flow cytometry revealed that *PAX5* overexpression did not affect the proportion of $CD3^+CD20^+$ T cells (Figure 8B and Supplemental Figure 22B). Therefore, we hypothesized that epigenetic processes may also regulate $CD20^+$ T cell differentiation and function. To investigate whether epigenetic mechanisms contribute to the observed differential expression of CD20, we analyzed DNA methylation patterns in $CD20^+$ T cells and $CD20^-$ T cells. We isolated $CD3^+CD20^+$ T cells, $CD3^+CD20^-$ T cells, and $CD19^+$ B cells from five healthy donors and conducted amplicon bisulfite sequencing to analyze DNA methylation levels across the *MS4A1* gene. The results revealed that differences in methylation levels among these cell populations were primarily attributed to differential methylation in the promoter region of *MS4A1* (Figure 8, C and D). Specifically, compared with $CD3^+CD20^+$ T cells, $CD3^+CD20^-$ T cells exhibited higher methylation levels at certain loci within the *MS4A1* promoter, such as -82 and +49 relative to the transcription start site (Figure 8E). Given the altered promoter

methylation levels observed in $CD20^+$ T cells, we introduced decitabine, a DNA methyltransferase (DNMT) inhibitor, into our coculture system. Our results revealed that DNMT inhibitor treatment increased CD20 expression in T cells overexpressing *PAX5* in vitro (Figure 8, F and G and Supplemental Figure 22C), suggesting that DNA methylation and PAX5 jointly regulate $CD20^+$ T cell development. These findings indicate that DNMT-mediated DNA methylation regulates the differentiation fate of $CD20^+$ T cells.

DISCUSSION

In this study, we identify $CD20^+$ T cells as a previously underappreciated component of the adaptive immune response in BP and provide evidence that these cells contribute to pathogenic humoral autoimmunity. We found that $CD20^+$ T cells were expanded in both the peripheral blood and skin lesions of patients with BP, and that their abundance correlated with serum anti-BP180 autoantibody titers and disease activity. While previous research has revealed correlations between $CD20^+$ T cells and autoimmune or viral diseases, their functions, transcriptional profiles, and origins in humans have remained poorly defined. We show that $CD20^+$ T cells are enriched for antigen-specific T cells, display increased proliferative, metabolic, and proinflammatory activity, and comprise functionally distinct $CD4^+$ and $CD8^+$ subsets. In particular, $CD4^+CD20^+$ T cells exhibit a pronounced Tfh-like phenotype and promote B cell differentiation and autoantibody production, whereas $CD8^+CD20^+$ T cells display predominantly cytotoxic and proinflammatory features. Mechanistically, we further show that *MS4A1* is endogenously expressed in T cells and is regulated by DNA methylation and the transcription factor PAX5. Our study identifies $CD20^+$ T cells as an important pathogenic adaptive immune component in BP and suggests that these cells may contribute to disease amplification and humoral autoimmunity.

One important advance of the present study is the demonstration that $CD20^+$ T cells are present not only in the circulation, but also within BP lesional skin and blister fluid. $CD20^+$ T cells have previously been described in the blood and in various tissues such as the thymus, bone marrow, secondary lymphoid organs, cerebrospinal fluid, and brain tissue (3, 22, 26). However, their presence within the tissue microenvironment of autoimmune blistering disease has not been demonstrated previously. The enrichment of these cells in BP lesions suggests that they are actively recruited to sites of inflammation and may participate directly in local immune amplification. In this regard, our data indicate that lesional $CD20^+$ T cells in BP are predominantly $CD4^+$ T cells, in contrast to the predominance of $CD8^+CD20^+$ T cells described in central nervous system lesions of multiple sclerosis (29). This disease-specific difference reinforces the notion that $CD20^+$ T cells are a heterogeneous compartment whose functional polarization is shaped by inflammatory context. In BP, our findings suggest that the lesional environment favors the accumulation of a $CD4^+$ Tfh-skewed $CD20^+$ subset, rather than a predominantly cytotoxic $CD8^+$ population.

T cells are central to autoimmune processes, where the breakdown of self-tolerance can lead to the production of autoantibodies, inflammation, and tissue infiltration by immune cells, ultimately resulting in the onset of autoimmune diseases (30). In this study, we show that $CD20^+$ T cells in BP are enriched for autoreactive cells and display heightened effector responsiveness. Using peptide stimulation assays and peptide-MHC class II tetramer staining, we found that the $CD4^+CD20^+$ subset was enriched for BP180-NC16A-reactive T cells. In contrast to conventional T cells, $CD20^+$ T cells in BP exhibited increased proliferative capacity and proinflammatory responses to autoantigens, characterized by increased production of cytokines, including IL-4, IL-17, and IFN-γ, which is consistent with observations in other autoimmune diseases (4, 7, 31).

These findings extend previous correlative studies by showing that $CD20^+$ T cells in BP are not passive bystanders but rather a highly responsive autoreactive population capable of amplifying both autoimmune and inflammatory responses.

Our additional single-cell RNA-seq analyses, together with complementary flow cytometric phenotyping, show that $CD20^+$ T cells are not a uniform population. Instead, $CD4^+CD20^+$ T cells preferentially express molecules associated with B cell help and Tfh-like programming, including PD-1, CXCR5, BCL6, MAF, and IL-21, whereas $CD8^+CD20^+$ T cells are enriched for activation and cytotoxic pathways and express higher levels of IFN-γ, granzyme B, and perforin. This distinction is important, because it places the pathogenic relevance of $CD20^+$ T cells in BP primarily within the $CD4^+$ subset, while still acknowledging that the $CD8^+$ subset may contribute to tissue inflammation through cytotoxic and proinflammatory mechanisms. More broadly, these data support the idea that $CD20^+$ T cells exhibit context-dependent functional plasticity across diseases. In multiple sclerosis, $CD20^+$ T cells have been reported to display a predominantly Th1/Tc1-like phenotype (22), whereas in rheumatoid arthritis they are enriched for $CXCR5^+PD\text{-}1^+$ T follicular helper and $CXCR5^-PD\text{-}1^+$ peripheral helper states (7). Our data indicate that in BP, $CD20^+$ T cells are functionally biased toward a Tfh-like B-cell helper program, particularly within the $CD4^+$ subset.

Although our data support a clear Tfh-like bias in $CD4^+CD20^+$ T cells, we intentionally define this population as Tfh-like rather than canonical Tfh cells. In addition to expressing PD-1, CXCR5, BCL6, MAF, and IL-21, these cells also retain features associated with other helper T-cell programs, including Th1 and Th17-related signatures. Such functional overlap is not unexpected in chronic autoimmune inflammation and is consistent with the concept of hybrid helper T-cell states in inflamed tissues. Despite this heterogeneity, our data strongly support a dominant B-cell-

helper role for $CD4^+CD20^+$ T cells in BP. These cells were preferentially enriched in BP skin lesions, promoted germinal center B cell differentiation, plasma cell generation, and autoantibody production more efficiently than $CD4^+CD20^-$ or $CD8^+CD20^+$ T cells in both ex vivo coculture and adoptive transfer assays, and their B-cell-helper activity was markedly attenuated by IL-21 neutralization in vivo. Together, these findings strengthen the mechanistic link between the Tfh-like phenotype of $CD4^+CD20^+$ T cells and their pathogenic B-cell-helper function in BP.

Although $CD20^+$ T cells were identified in the 1990s, their origin remains contentious. Recent research highlights the role of trogocytosis, the process of transferring intact membrane patches between cells, in modulating immune responses, particularly between T cells and antigen-presenting cells (32). For example, de Bruyn et al. demonstrated that HLA-DR and CD20 are rapidly transferred from B cells to T cells (within 15 minutes) during coculture experiments (31). Additionally, studies using mouse models have shown that T cells can acquire CD20 from CD20-expressing B cells through direct contact, supporting the trogocytosis hypothesis (4). However, $CD20^+$ T cells may also express CD20 endogenously. In our study, we found that $CD20^+$ T cells isolated from human peripheral blood expressed *MS4A1* mRNA, which is consistent with previous findings that human T cells can transcribe *MS4A1* and synthesize CD20 themselves (25, 26, 33). Additionally, another study reported that $CD3^+CD20^+$ T cells do not express HLA-DR, a molecule typically transferred to T cells during trogocytosis (26). Furthermore, our bulk RNA-seq analysis revealed low or no expression of other membrane proteins associated with CD20, such as HLA-DR, CD40, and CD81, in $CD20^+$ T cells, suggesting that CD20 is endogenously expressed rather than acquired via trogocytosis. Studies involving lymph node T cells from monkeys revealed a marked increase in *MS4A1* mRNA expression when these cells were stimulated with mitogens and IL-2 in vitro, suggesting that the cellular microenvironment plays a crucial role in regulating CD20

expression (34). Our results demonstrated that CD20 expression on $CD20^+$ T cells is upregulated following TCR activation, independently of the presence of B cells. Thus, our data support the view that at least a subset of $CD20^+$ T cells can endogenously express CD20, rather than acquiring it solely through trogocytosis.

PAX5 is a crucial transcription factor involved in lineage commitment and identity, particularly in B cells and T cells (28, 35). Loss of PAX5 can reprogram pro-B cells into hematopoietic progenitors with the potential to differentiate into various cell types, including myeloid cells, macrophages, granulocytes, osteoclasts, natural killer cells, and T cells (28, 36). These findings underscore the important role of PAX5 in immune cell development. Aberrant expression of PAX5 has been implicated in primary cutaneous T-cell lymphomas (37), and experimental models have demonstrated that PAX5 overexpression can induce T-cell neoplasms (38). Our study revealed that PAX5 was expressed in $CD20^+$ T cells, that the *MS4A1* regulatory region contained a predicted PAX5-binding motif, and mutation of this site reduced reporter activity. In parallel, TCR stimulation induced PAX5 expression, followed by increased CD20 expression, supporting activation-dependent engagement of the PAX5-CD20 axis in T cells. Consistent with this model, *PAX5* deficiency reduced CD20 expression, decreased the frequency of $CXCR5^+PD\text{-}1^+$ cells and lowered IL-21 production. These findings suggest that PAX5 helps sustain the activation state of $CD20^+$ T cells and reinforces their Tfh-like features, although it is unlikely to act as the sole determinant of Tfh lineage commitment.

In addition to transcription factors, epigenetic mechanisms are crucial for regulating CD20 expression, particularly in B cells, and involve processes such as histone acetylation and DNA methylation (1). Previous studies have shown that treatment with histone deacetylase (HDAC) inhibitors, such as trichostatin A (39), and DNMT inhibitors, such as 5-aza-2-deoxycytidine (40),

can increase CD20 mRNA and protein levels in B cells. In our study, we found that $CD20^+$ T cells have lower DNA methylation levels in the *MS4A1* promoter region than do $CD20^-$ T cells. These findings suggest that in $CD20^+$ T cells, this region has increased accessibility to transcription factors. Interestingly, overexpressing *PAX5* alone did not result in an increase in CD20 expression. However, when *PAX5* overexpression was combined with DNMT inhibitor treatment, CD20 expression in T cells was markedly increased. These findings indicate that DNMT inhibition reduces the methylation of the *MS4A1* promoter, thereby facilitating greater PAX5 binding to the promoter and promoting *MS4A1* transcription and translation. These results highlight the complex interplay between epigenetic modifications and transcription factor regulation in $CD20^+$ T cell biology.

Anti-CD20 therapy is commonly used to treat B cell lymphoma and autoimmune disorders. CD20 positivity renders this pathogenic $CD20^+$ T cell population susceptible to anti-CD20 therapy. Multiple studies have found that RTX treatment not only efficiently depletes $CD20^+$ B cells from the blood but also eliminates the $CD20^+$ T cell subset. Both cell types reappear after discontinuation of anti- CD20 antibodies and $CD20^+$ T cells reappear in the peripheral blood earlier than B cells (4). In addition, we found that JAK-STAT signaling was enriched in $CD4^+CD20^+$ T cells, and that baricitinib reduced the frequency of $CD20^+$ T cells and suppressed Tfh-related effector functions, including IL-21 and IFN-γ production (Supplemental Figure 23). These observations raise the possibility that pathogenic $CD20^+$ T cells may be targeted either through CD20-directed depletion or by inhibiting upstream signaling pathways that sustain their activation and effector function.

Study limitations. Although our active immunization model reproduced the major serologic and immunopathologic features of BP, including anti-BP180 autoantibodies and linear IgG/C3

deposition at the dermal-epidermal junction, it did not consistently generate overt blistering and therefore does not fully recapitulate all clinical aspects of human disease. Likewise, adoptive transfer of $CD4^+CD20^+$ T cells together with B cells into $Rag1^{-/-}$ mice enhanced B cell differentiation and antibody production, but did not induce overt BP-like disease, indicating that this system is best interpreted as a model of pathogenic B-cell help rather than complete disease transfer. In addition, we did not perform T cell-specific conditional deletion of CD20 or PAX5 in vivo, nor did we generate a mouse single-cell transcriptomic atlas to more precisely resolve the heterogeneity and lineage relationships of $CD20^+$ T cell subsets in the BP model. These issues will need to be addressed in future studies to define the in vivo functions and therapeutic potential of these cells more precisely.

In conclusion, our study identifies $CD20^+$ T cells as a pathogenic adaptive immune component in BP and reveals that $CD4^+CD20^+$ T cells constitute a Tfh-like, antigen-reactive B cell helper subset that promotes B cell differentiation and autoantibody production, whereas $CD8^+CD20^+$ T cells are biased toward cytotoxic and proinflammatory functions. We further show that CD20 is endogenously expressed in T cells and is regulated by DNA methylation and PAX5, thereby defining a previously unrecognized regulatory program associated with pathogenic T cell activation in BP. These findings not only expand our understanding of CD20 biology beyond the B cell lineage, but also nominate $CD20^+$ T cells and their associated signaling pathways as potential therapeutic targets in BP.

MATERIALS AND METHODS

Sex as a biological variable

Female SJL/J mice were used in this study. As previously reported, female SJL/J mice are more susceptible than males to the induction of BP-like skin lesions and phenotypes (24).

Human samples

Peripheral blood, BF, and skin tissues were collected from BP patients at the Department of Dermatology, Xijing Hospital. The study included 36 untreated patients (mean age: 69 years, range: 51–87) and 35 healthy controls (mean age: 60 years, range: 48–69). Healthy controls were frequency-matched for sex and broadly age-matched. The detailed patient characteristics are provided in Supplemental Tables 1 and 2. BP diagnoses were confirmed on the basis of typical clinical and histological presentations, direct or indirect immunofluorescence examinations, and detection of circulating autoantibodies against BP180-NC16A. All enrolled participants developed blisters within 1 month and had not received systemic or topical immunosuppressive treatments before blood sample collection. Ten patients each with pemphigus vulgaris, psoriasis, and lichen planus donated skin lesions for tissue immunofluorescence. Healthy controls were selected to match patients in terms of sex and age, and none exhibited signs of chronic autoimmune diseases or acute infections in their blood samples. Peripheral blood mononuclear cells (PBMCs) were isolated from blood samples using human lymphocyte separation medium with Ficoll gradient centrifugation (Dakewei, Shenzhen, China) following the manufacturer's instructions. BF was collected in an ice bath and immediately centrifuged for 10 min at 300 × g to separate the cells from the BF. HLA typing was conducted via Sanger sequencing of the second exon at BGI LifeTech, China.

Mice

SJL/J mice (8–10 weeks old) were purchased from Beijing Vital River Laboratory Animal Technology Company. The mice were immunized with a recombinant form of the immunodominant 15th noncollagenous domain of murine BP180 as previously described (24). Briefly, each mouse was injected subcutaneously in the hind footpad with 60 μg of murine BP180 protein (fused with GST; Proteintech Group) emulsified in the nonionic block copolymer adjuvant TiterMax (Sigma-Aldrich, H4397). Boost immunizations were administered twice at 3-week intervals. Negative control mice were immunized with TiterMax alone. After 4 weeks, biopsies were obtained from nonlesional skin to assess IgG and C3 deposits at the epidermal–dermal junction. Immune cells isolated from blood, lymph nodes, and spleen were stained with fluorochrome-labeled antibodies and analyzed using FlowJo software. Peripheral blood was collected by retro-orbital bleeding under anesthesia.

For the adoptive T cell transfer mouse model, recipient $Rag1^{-/-}$ mice (6–8 weeks old) were obtained from Chengdu Yaokang Biotechnology company. Donor single-cell suspensions were prepared from the spleens and lymph nodes of BP180-immunized mice harvested 4 weeks post-immunization. The tissues were mechanically dissociated through a 70- μm cell strainer in RPMI 1640 medium supplemented with 10% FBS, streptomycin (100 μg/ml), penicillin G (100 U/ml), and l-glutamine (0.3 mg/ml). Single cells were subsequently stained with antibodies, followed by sorting of $CD4^+CD20^+$, $CD8^+CD20^+$, and $CD4^+CD20^-$ T cells using a MoFLO XDP (Beckman Coulter) flow cytometer. Magnetically labeled B cells were isolated using a B-cell isolation kit (Miltenyi Biotech, 130-090-862). For adoptive transfer, sorted T cells from each subset, along with 1×10^6 B cells, were intravenously injected into the $Rag1^{-/-}$ recipients. In a parallel cohort, a separate group of $Rag1^{-/-}$ mice receiving adoptive transfer of $CD4^+CD20^+$ T cells was concurrently administered an anti-IL-21 neutralizing antibody (100 μg per mouse, Invitrogen, Cat# 16-7211-85)

via tail vein injection on day 0. Fourteen days after transfer, the skin, spleens, and serum were harvested from recipient mice for subsequent analysis.

scRNA-seq and data analysis

Single-cell RNA sequencing libraries were constructed using the 10x Genomics Chromium Single Cell 3′ Library & Gel Bead Kit v3.1 according to the manufacturer's protocol and sequenced on the Illumina NovaSeq 6000 platform. The raw sequencing data were processed using Cell Ranger (v6.1.2, 10x Genomics). The FASTQ files were aligned to the human reference genome GRCh38 (hg38), and gene expression matrices were generated based on unique molecular identifiers (UMIs). Subsequent analyses were conducted using the Seurat package (v5.2.1) in R. Cells with fewer than 200 or more than 4,000 detected genes, total UMI counts exceeding 20,000, mitochondrial gene percentages greater than 10%, or hemoglobin gene percentages greater than 10% were excluded. The filtered data were then normalized using the "LogNormalize" method. Highly variable genes (n = 2,000) were identified using the "vst" method, and the data were scaled prior to dimensionality reduction. Principal component analysis was performed on the highly variable genes. For batch correction and data integration across samples, Harmony-based integration was applied using the IntegrateLayers function with the first 20 principal components. The integrated object was joined with JoinLayers, and subsequent dimensionality reduction was conducted via UMAP using the top 15 Harmony components. Cell types were annotated based on the expression of canonical marker genes. $CD20^+$ T cells were identified as a subset of T lymphocytes co-expressing canonical T cell markers (e.g., *CD3D*, *CD3E*, *CD4*, and *CD8A*) and *MS4A1*. A threshold for *MS4A1* expression was applied to distinguish $CD20^+$ from $CD20^-$ T cells, and the resulting $CD20^+$ T cell population was extracted from the Seurat object for downstream

analyses, including differential gene expression, functional enrichment, and cell–cell communication analyses. To investigate intercellular communication among different cell types, we used the CellChat R package (version 2.1.2). Cell–cell interactions were inferred based on known ligand–receptor pairs. Specifically, the netVisual heatmap function was used to visualize the interaction strengths between $CD20^+$ T cells and other immune cell populations.

Bulk RNA sequencing

Total RNA extracted from the peripheral $CD3^+CD20^+$ T cells, $CD3^+CD20^-$ T cells, and $CD19^+$ B cells of BP patients (n = 3) and age- and sex-matched healthy controls (n = 3) was subjected to deep sequencing on an Illumina NovaSeq platform (Gene Denovo Biotechnology Corporation). Raw sequencing reads were processed and mapped to the human reference genome, and gene-level raw counts were obtained. Differential gene expression analysis was performed using the DESeq2 R package based on raw count data. Genes with an absolute fold change $\geqslant 1.5$ and adjusted P value < 0.05 were considered DEGs. For visualization purposes, gene expression levels were normalized as fragments per kilobase of transcript per million mapped reads (FPKM). Expression profiles and plots were generated using Omicsmart tools. Functional enrichment analyses of DEGs were performed using GO and KEGG databases with the R packages clusterProfiler, org.Hs.eg.db, enrichplot, and ggplot2.

Tissue and cell immunofluorescence staining

For the skin tissue samples, 4-μm sections of the paraffin-embedded skin samples were deparaffinized and rehydrated. After being blocked with 5% goat serum for 30 min at room temperature, the skin sections were incubated with primary antibodies overnight at 4°C. The

following antibodies were used: rat monoclonal CD3 (Abcam, Cat# ab11089), rat monoclonal CD4 (Santa Cruz, Cat# sc-13573), mouse monoclonal CD20 (Abcam, Cat# ab9475), rabbit monoclonal CD20 (Abcam, Cat# ab78237), rabbit monoclonal CD19 (Abcam, Cat# ab134114), and mouse monoclonal CD8 (Abcam, Cat# ab316355). After being washed three times with PBS, the skin tissues were incubated with Cy5-conjugated goat anti-rat IgG (Abcam, Cat# ab6565), Cy3-conjugated goat anti-mouse IgG (Abcam, Cat# ab97035), Cy3-conjugated goat anti-rabbit IgG (Abcam, Cat# ab6939), Alexa Fluor 488-conjugated goat anti-mouse IgG (Abcam, Cat# ab150113) or Alexa Fluor 488-conjugated goat anti-rabbit IgG (Abcam, Cat# ab150077) as secondary antibodies. Nuclear DNA was detected by incubating the sections with Hoechst 33258 (Solarbio Technology, C0021) for 10 min at room temperature. Images were acquired using a Zeiss LSM 880 confocal microscope (Zeiss Optotechnik GmbH).

For cell immunofluorescence staining, $CD3^+CD20^+$ T cells, $CD3^+CD20^-$ T cells and $CD19^+$ B cells were isolated from healthy controls via flow cytometry. The suspended cells were seeded on poly-L-lysine-coated coverslips, fixed immediately with 4% paraformaldehyde for 15 min, and permeabilized with 0.25% Triton X-100 (Beyotime, Cat# P0096) at room temperature. The cells were blocked with 5% goat serum for 30 min and then incubated with primary antibodies, including rat monoclonal CD3 (Abcam, Cat# ab11089), mouse monoclonal CD20 (Abcam, Cat# ab9475), and rabbit monoclonal PAX5 (Abcam, Cat# ab109443) antibodies at 4 °C overnight. After incubation with the corresponding secondary antibodies and Hoechst 33258, the cells were observed with a confocal microscope (LSM880, Carl Zeiss).

Flow cytometry analysis

PBMCs were incubated in FcR blocking reagent (Miltenyi Biotec, 130-059-091) to prevent nonspecific antibody binding and subsequently stained for 30 minutes at 4°C with fluorophore-conjugated antibodies. The following antibodies were used: APC anti-human CD3 antibody (BioLegend, Cat# 300312), PE/Cyanine7 anti-human CD4 antibody (BioLegend, Cat# 357410), BV605 anti-human CD4 antibody (BioLegend, Cat# 317438), PerCP/Cyanine5.5 anti-human CD8 antibody (BioLegend, Cat# 344710), FITC anti-human CD8 antibody (BioLegend, Cat# 344704), FITC anti-human CD19 antibody (BioLegend, Cat# 363008), PE anti-human CD20 antibody (BioLegend, Cat# 302306), PE/Cyanine7 anti-human CD20 antibody (BioLegend, Cat# 302312), PE anti-human CXCR5 antibody (BioLegend, Cat# 356904), PerCP/Cyanine5.5 anti-human CXCR5 antibody (BioLegend, Cat# 356910), Pacific Blue anti-human PD-1 antibody (BioLegend, Cat# 329916), PerCP/Cyanine5.5 anti-PAX5 antibody (BioLegend, Cat# 649710), PE anti-human IFN-γ antibody (BioLegend, Cat# 506507), FITC anti-human IL-4 antibody (BioLegend, Cat# 500806), Brilliant Violet 605 anti-human IL-17A antibody (BioLegend, Cat# 512326), PerCP/Cyanine5.5 anti-human IL-21 antibody (BioLegend, Cat# 513012), PE anti-human Perforin Antibody (BioLegend, Cat# 308106) and FITC anti-human/mouse Granzyme B Antibody (BioLegend, Cat# 515403) .

Murine immune cells were stained with APC anti-mouse CD3 antibody (BioLegend, Cat# 100236), PE/Cyanine7 anti-mouse CD4 antibody (BioLegend, Cat# 100422), BV421 anti-mouse CD4 antibody (BioLegend, Cat# 100438), PerCP/Cyanine5.5 anti-mouse CD8a antibody (BioLegend, Cat# 100734), BV605 anti-mouse CD8a antibody (BioLegend, Cat# 100744), FITC anti-mouse CD19 antibody (BioLegend, Cat# 115506), PE anti-mouse CD20 antibody (BioLegend, Cat# 150410), Alexa Fluor 488 anti-mouse B220 antibody (BioLegend, Cat# 103227), Pacific Blue anti-mouse GL7 antibody (BioLegend, Cat# 144614), APC anti-mouse Fas antibody

(BioLegend, Cat# 152604), PE/Cyanine7 anti-mouse PD-1 antibody (BioLegend, Cat# 135216), BV605 anti-mouse CXCR5 antibody (BioLegend, Cat# 145513), AF488 anti-mouse IL-21 antibody (R&D Systems, Cat# IC594G), PE/Cyanine7 anti-mouse IgD antibody (BioLegend, Cat# 405720), APC/Cyanine7 anti-mouse CD138 (Syndecan-1) antibody (BioLegend, Cat# 142530), and Zombie UV dye (BioLegend, Cat# 423102) in FACS buffer for 30 min and then analyzed by flow cytometry (BD LSRFortessa Cell Analyzer). Isotype-matched controls were used to correct for nonspecific antibody binding and spectral overlap, where appropriate. For cytokines, cells were stimulated with PMA and ionomycin with the protein transport inhibitor BD GolgiPlug (BD Biosciences, 550583) at 37°C and 5% CO_2 for 6 hours. For intracellular staining, the cells were fixed and permeabilized using the Cytofix/Cytoperm Fixation/Permeabilization Solution Kit (BD Biosciences, 554714) or Foxp3/Transcription Factor Staining Buffer Set (eBioscience, 00-5523-00) and stained with fluorescent antibodies for an additional 30 minutes at 4°C in the dark. Data analysis was performed using FlowJo software.

Tetramer flow cytometry

PBMCs were isolated from BP patients and healthy controls, and then, the cells (2×10^5 cells per well) were seeded into 96-well U-bottom plates and cultured in RPMI 1640 medium (Gibco) supplemented with 10% fetal bovine serum and streptomycin (100 μg/ml), penicillin G (100 U/ml), and L-glutamine (0.3 mg/ml). PBMCs were stimulated in duplicate using peptide pools (1 μM/well for each peptide) and 20 U/mL recombinant human IL-2 (R&D Systems) at 37°C with 5% CO_2 for 5 days. Anti-CD3/CD28 Dynabeads (Gibco, 11141D) were used as positive controls to monitor T cell expansion. For a negative control, unstimulated cells were included on each plate.

A PE-labeled ProT2 MHC Tetramer (HLA-DRA1*01:01/DRB1*15:01 ELERIRRSILPYGDS) was constructed by PROIMMUNE. For MHC tetramer staining, two microliters of tetramer were added to each tube and incubated at room temperature for 1 hour, followed by one wash in 15 mL of cold sorting buffer (PBS with 2% FBS and 0.1% NaN_3) and centrifugation at 300 × g for 5 minutes. For antibody staining, enriched tetramer-binding PBMCs were incubated for 30 minutes at 4°C with APC-conjugated CD3 antibody, BV605-conjugated CD4 antibody, and PE-Cy7-conjugated CD20 antibody against surface markers. The cells were washed and fixed in 2% paraformaldehyde in PBS overnight at 4°C. Single-stained compensation controls were used for spectral compensation. Fluorescence-minus-one controls and/or isotype controls were used where appropriate for gate setting. Tetramer-positive T cells were identified based on their binding to the pMHC II tetramer. The samples were analyzed with a BD LSRFortessa flow cytometer.

Ex vivo co-culture assay

On day 28 following BP180 immunization, $CD4^+CD20^+$ T cells, $CD4^+CD20^-$ T cells, and $CD8^+CD20^+$ T cells were isolated from the mouse spleen and lymph nodes via fluorescence-activated cell sorting. Magnetically labeled B cells were isolated using a B-cell isolation kit (Miltenyi Biotec, 130-090-862). Subsequently, each of the three T-cell subsets was co-cultured with B cells at a 1:1 ratio in media supplemented with anti-CD3/CD28 Dynabeads and IL-2. T cell subsets were seeded at a density of 1×10^5 cells per well in a 96-well plate. Following 7 days of incubation, cells were harvested for the analysis of B-cell differentiation, and culture supernatants were collected for the measurement of antibody titers by enzyme-linked immunosorbent assay.

Cell culture and lentiviral transduction

For PAX5 overexpression, lentiviral constructs carrying the PAX5 gene or a negative control sequence were generated and packaged by Tsingke Biotechnology. Human primary T cells were extracted from PBMCs using a Pan T isolation kit (Miltenyi Biotec, 130-096-535). First, T cells (2.0×10^5 per well) were activated with anti-CD3/CD28 Dynabeads at a 1:1 ratio in 500 μL of RPMI 1640 medium supplemented with 10% FBS and human rIL-2 (30 IU/mL) in 48-well plates. After 24 h, 2×10^7 TU of ZsGreen-Puro/CMV-PAX5 or negative control lentivirus in complete RPMI 1640 supplemented with rIL-2 and 8 μg/mL polybrene were added to the cell suspension at a final volume of 750 μL at a multiplicity of infection (MOI) of 100 for 12 h. Then, the cells were harvested and incubated in RPMI 1640 culture medium supplemented with 10% FBS, antibiotics, rhIL-2 and anti-CD3/CD28 Dynabeads in 48-well plates for 72 h. To inhibit promoter methylation in T cells, a 10 μM concentration of the DNMT inhibitor decitabine (MedChemExpress, HY-A0004) was used to pretreat the culture system. After culture, the cells were expanded, and the expression of PAX5 and MS4A1 was evaluated via RT-qPCR.

PAX5 knockout in primary human T cells and *MS4A1* knockout in primary mouse T cells were performed via the CRISPR–Cas9 system. The cutting efficiency of each CRISPR guide RNA construct was validated by transfecting HEK293T cells (Fuheng Biology) and sequencing the target regions in the genome. Recombinant *PAX5* knockout lentiviruses and *MS4A1* knockout lentiviruses were synthesized by Tsingke Biotechnology and transduced into primary human or mouse T cells as described above.

Statistics

Each experiment was performed at least 3 times. All the data are presented as the mean ± SD. Statistical analyses of the data were performed using GraphPad Prism (version 9.0.2) and R. Two-tailed paired and unpaired Student's t tests and one-way and two-way ANOVA were used to evaluate the statistical significance of differences among groups. Correlation analysis was performed via Spearman's rank correlation test. $P < 0.05$ was considered to indicate statistical significance.

Study approval

All procedures involving the use of human samples were performed in accordance with institutional guidelines and with approval from the Ethical Committee of Xijing Hospital of the Fourth Military Medical University. Written informed consent was obtained from all participants prior to sample collection. All animal experiments were performed according to institutional guidelines and were approved by the Review Committee for the Use of Animals of the Fourth Military Medical University.

Data availability

The accession numbers for the sequencing raw data in this paper are GSA (Genome Sequence Archive in BIG Data Center, Beijing Institute of Genomics, Chinese Academy of Sciences): HRA008361 and HRA018190. Values for all data points in graphs are reported in the Supporting Data Values file.

Additional materials and methods are provided in the online Supplemental Materials and Methods.

Author contributions

HF, SXS, SS, ED and GW conceived the project and designed the experiments. HF, SXS, KL, TC, BW, HM, KX, LL, XL and YB performed the experiments and data analyses. PQ, JZ, CZ, CX, and BP provided technical assistance. GW, HF, SS and HHQ obtained the funding for this study. HF and SXS wrote the manuscript with input and revision from GW, ED, SS, MF and HJQ. All the authors read and approved the final manuscript.

Funding support

This work was supported by the National Key R&D Program of China (2022YFC3601800 to GW), the National Natural Science Foundation of China (82173410 to HF; 82322057 to SS), and the Natural Science Foundation of Shaanxi Province, China (2024JC-YBQN-0772 to HHQ).

Acknowledgments

We would like to thank our patients and healthy volunteers for their enthusiastic participation. We would also like to thank Meihong Yu, Na Li, Yi Wang, and Qiaozhen Lin for their assistance with the immunofluorescence staining.

References

1. Pavlasova G, and Mraz M. The regulation and function of CD20: an "enigma" of B-cell biology and targeted therapy. *Haematologica.* 2020;105(6):1494-506.
2. Hultin LE, et al. CD20 (pan-B cell) antigen is expressed at a low level on a subpopulation of human T lymphocytes. *Cytometry.* 1993;14(2):196-204.
3. Holley JE, et al. CD20+inflammatory T-cells are present in blood and brain of multiple sclerosis patients and can be selectively targeted for apoptotic elimination. *Mult Scler Relat Disord.* 2014;3(5):650-8.

4. Ochs J, et al. Proinflammatory CD20(+) T cells contribute to CNS-directed autoimmunity. *Sci Transl Med.* 2022;14(638):eabi4632.
5. Quendt C, et al. Proinflammatory CD20(+) T Cells are Differentially Affected by Multiple Sclerosis Therapeutics. *Ann Neurol.* 2021;90(5):834-9.
6. Eggleton P, et al. Frequency of Th17 CD20+ cells in the peripheral blood of rheumatoid arthritis patients is higher compared to healthy subjects. *Arthritis Res Ther.* 2011;13(6):R208.
7. Pan P, et al. Aberrant pro-inflammatory responses of CD20(+) T cells in experimental arthritis. *Cell Immunol.* 2023;387:104717.
8. Alunno A, et al. Interleukin (IL)-17-producing pathogenic T lymphocytes co-express CD20 and are depleted by rituximab in primary Sjögren's syndrome: a pilot study. *Clin Exp Immunol.* 2016;184(3):284-92.
9. Niu J, et al. Dissection of a circulating CD3(+) CD20(+) T cell subpopulation in patients with psoriasis. *Clin Exp Immunol.* 2018;192(2):206-12.
10. Pinho ACO, et al. Identification and characterization of circulating and adipose tissue infiltrated CD20(+)T cells from subjects with obesity that undergo bariatric surgery. *Immunol Lett.* 2024;269:106911.
11. Rodrigues C, et al. CD20+ T cells in monoclonal B cell lymphocytosis and chronic lymphocytic leukemia: frequency, phenotype and association with disease progression. *Front Oncol.* 2024;14:1380648.
12. de Sèze J, et al. Anti-CD20 therapies in multiple sclerosis: From pathology to the clinic. *Front Immunol.* 2023;14:1004795.
13. Pisetsky DS. Pathogenesis of autoimmune disease. *Nat Rev Nephrol.* 2023;19(8):509-24.
14. Sun L, et al. T cells in health and disease. *Signal Transduct Target Ther.* 2023;8(1):235.
15. Hammers CM, and Stanley JR. Mechanisms of Disease: Pemphigus and Bullous Pemphigoid. *Annu Rev Pathol.* 2016;11:175-97.
16. Zhang J, et al. Identification of Immunodominant Th2-Cell Epitopes in Chinese Patients with Bullous Pemphigoid. *J Invest Dermatol.* 2018;138(9):1917-24.
17. Liu T, et al. Single-cell transcriptomics analysis of bullous pemphigoid unveils immune-stromal crosstalk in type 2 inflammatory disease. *Nat Commun.* 2024;15(1):5949.
18. Chakievska L, et al. IL-17A is functionally relevant and a potential therapeutic target in

bullous pemphigoid. *J Autoimmun.* 2019;96:104-12.
19. Li Q, et al. Follicular helper T Cells (Tfh) and IL-21 involvement in the pathogenesis of bullous pemphigoid. *PLoS One.* 2013;8(7):e68145.
20. Haeberle S, et al. Regulatory T-cell deficiency leads to pathogenic bullous pemphigoid antigen 230 autoantibody and autoimmune bullous disease. *J Allergy Clin Immunol.* 2018;142(6):1831-42.e7.
21. Muramatsu K, et al. Regulatory T-cell dysfunction induces autoantibodies to bullous pemphigoid antigens in mice and human subjects. *J Allergy Clin Immunol.* 2018;142(6):1818-30.e6.
22. von Essen MR, et al. Proinflammatory CD20+ T cells in the pathogenesis of multiple sclerosis. *Brain.* 2019;142(1):120-32.
23. Crotty S. Follicular helper CD4 T cells (TFH). *Annu Rev Immunol.* 2011;29:621-63.
24. Hirose M, et al. Repetitive immunization breaks tolerance to type XVII collagen and leads to bullous pemphigoid in mice. *J Immunol.* 2011;187(3):1176-83.
25. Palanichamy A, et al. Rituximab efficiently depletes increased CD20-expressing T cells in multiple sclerosis patients. *J Immunol.* 2014;193(2):580-6.
26. Schuh E, et al. Features of Human CD3+CD20+ T Cells. *J Immunol.* 2016;197(4):1111-7.
27. Cobaleda C, et al. Pax5: the guardian of B cell identity and function. *Nat Immunol.* 2007;8(5):463-70.
28. Hagman J, and Lukin K. "Hands-on" regulation of B cell development by the transcription factor Pax5. *Immunity.* 2007;27(1):8-10.
29. von Essen MR, et al. Intrathecal CD8(+)CD20(+) T Cells in Primary Progressive Multiple Sclerosis. *Neurol Neuroimmunol Neuroinflamm.* 2023;10(5):e200140.
30. Fang H, et al. The role of T cells in pemphigus vulgaris and bullous pemphigoid. *Autoimmun Rev.* 2020;19(11):102661.
31. de Bruyn M, et al. CD20(+) T cells have a predominantly Tc1 effector memory phenotype and are expanded in the ascites of patients with ovarian cancer. *Oncoimmunology.* 2015;4(4):e999536.
32. Ahmed KA, et al. Intercellular trogocytosis plays an important role in modulation of immune responses. *Cell Mol Immunol.* 2008;5(4):261-9.
33. Mudd TW, Jr., et al. MS4A1 expression and function in T cells in the colorectal cancer

tumor microenvironment. *Cell Immunol.* 2021;360:104260.

34. Murayama Y, et al. Transient expression of CD20 antigen (pan B cell marker) in activated lymph node T cells. *Microbiol Immunol.* 1996;40(6):467-71.

35. Cotta CV, et al. Pax5 determines B- versus T-cell fate and does not block early myeloid-lineage development. *Blood.* 2003;101(11):4342-6.

36. Mikkola I, et al. Reversion of B cell commitment upon loss of Pax5 expression. *Science.* 2002;297(5578):110-3.

37. Hagiwara M, et al. Primary cutaneous CD30 positive T-cell lymphoproliferative disorders with aberrant expression of PAX5: report of three cases. *Pathol Int.* 2012;62(4):264-70.

38. Feldman AL, et al. PAX5-positive T-cell anaplastic large cell lymphomas associated with extra copies of the PAX5 gene locus. *Mod Pathol.* 2010;23(4):593-602.

39. Tomita A, et al. Epigenetic regulation of CD20 protein expression in a novel B-cell lymphoma cell line, RRBL1, established from a patient treated repeatedly with rituximab-containing chemotherapy. *Int J Hematol.* 2007;86(1):49-57.

40. Tsutsumi Y, et al. 5-Azacytidine partially restores CD20 expression in follicular lymphoma that lost CD20 expression after rituximab treatment: a case report. *J Med Case Rep.* 2016;10:27.

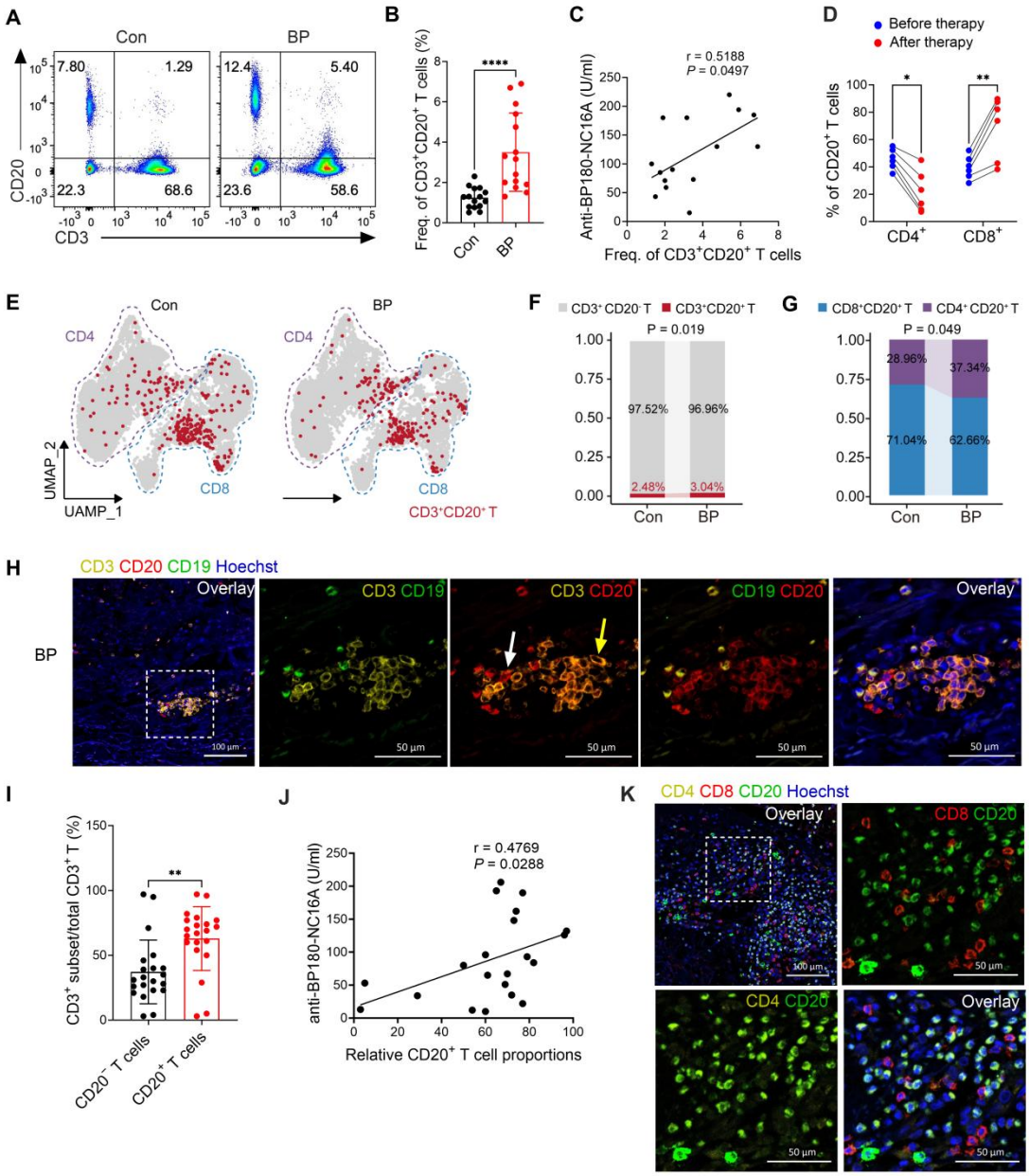

855

856 **Figure 1. Increased levels of CD20$^+$ T cells in patients with bullous pemphigoid (BP).** (**A**)
857 Representative flow cytometry dot plot showing CD3$^+$CD20$^+$ T cell identification in peripheral
858 blood. (**B**) Frequencies of CD3$^+$CD20$^+$ T cells in PBMCs from healthy controls (Con, n = 15) and
859 BP patients (n = 15). (C) Correlation between the proportions of circulating CD3$^+$CD20$^+$ T cells
860 and serum anti-BP180-NC16A antibody titers in BP patients (n = 15). (**D**) Frequencies of
861 CD4$^+$CD20$^+$ and CD8$^+$CD20$^+$ T cells before and after glucocorticoid treatment in BP patients (n =
862 6). (**E**) Uniform manifold approximation and projection (UMAP) visualization of CD3$^+$CD20$^+$ T
863 cells and subsets (CD4$^+$ and CD8$^+$) in Con and BP patients. (**F**) Bar charts showing the proportions
864 of CD3$^+$CD20$^+$ T cells in Con and BP patients. (**G**) Bar charts showing the proportions of
865 CD4$^+$CD20$^+$ and CD8$^+$CD20$^+$ T cells in Con and BP patients. (**H**) Representative images of
866 immunofluorescence staining for CD3 (yellow), CD19 (green), CD20 (red) and DNA (Hoechst,

blue) in the skin lesions of BP patients. Scale bar = 100 μm; scale bar insert = 50 μm. (**I**) Relative proportions of $CD3^+CD20^+$ and $CD3^+CD20^-$ T cells in the skin lesions of individual BP patients (n = 21). (**J**) Correlation between the relative proportions of $CD3^+CD20^+$ T cells in skin lesions and anti-BP180-NC16A antibody titers in BP patients (n = 21). (**K**) Representative images of immunofluorescence staining for CD4 (yellow), CD8 (red), CD20 (green) and DNA (Hoechst, blue) in BP skin lesions (n = 8). Scale bar = 100 μm; scale bar insert = 50 μm. All data are presented as the mean ± SD. An unpaired two-tailed Student's *t* test was used for B and I; Spearman's correlation was used for C and J; Chi-square test was used for F and G; a paired Student's t test was used for D. $^{**}P < 0.01$, $^{****}P < 0.0001$.

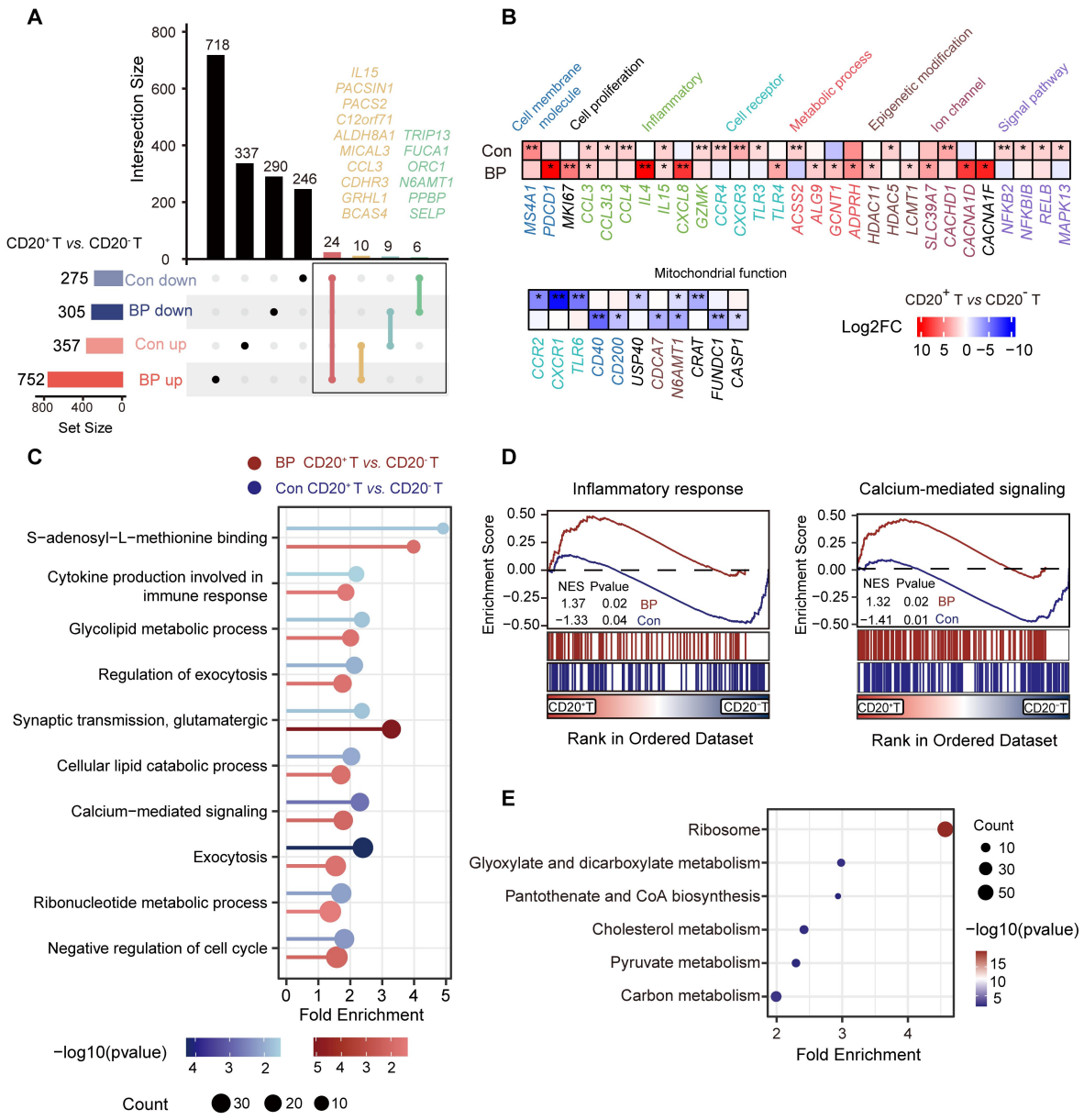

Figure 2. RNA sequencing analysis of CD20⁺ T cells in the peripheral blood of humans. $CD3^+CD20^+$ T cells, $CD3^+CD20^-$ T cells and B cells were sorted from 3 BP patients and 3 sex- and age-matched healthy controls (Con). (**A**) UpSet plot showing the overlap of differentially expressed genes (DEGs; upregulated and downregulated) between $CD20^+$ T and $CD20^-$ T cells in Con and BP patients. (**B**) Heatmap of DEGs between $CD20^+$ T cells and $CD20^-$ T cells from Con and BP patients. (**C**) Gene Ontology (GO) enrichment analysis of DEGs between $CD20^+$ and $CD20^-$ T cells in BP patients and Con. (**D**) Gene set enrichment analysis (GSEA) showing enrichment of genes sets associated with inflammatory response and calcium-mediated signaling in $CD20^+$ T cells. (**E**) Kyoto Encyclopedia of Genes and Genomes (KEGG) pathway enrichment of DEGs between $CD20^+$ T cells from BP patients and those from Con.

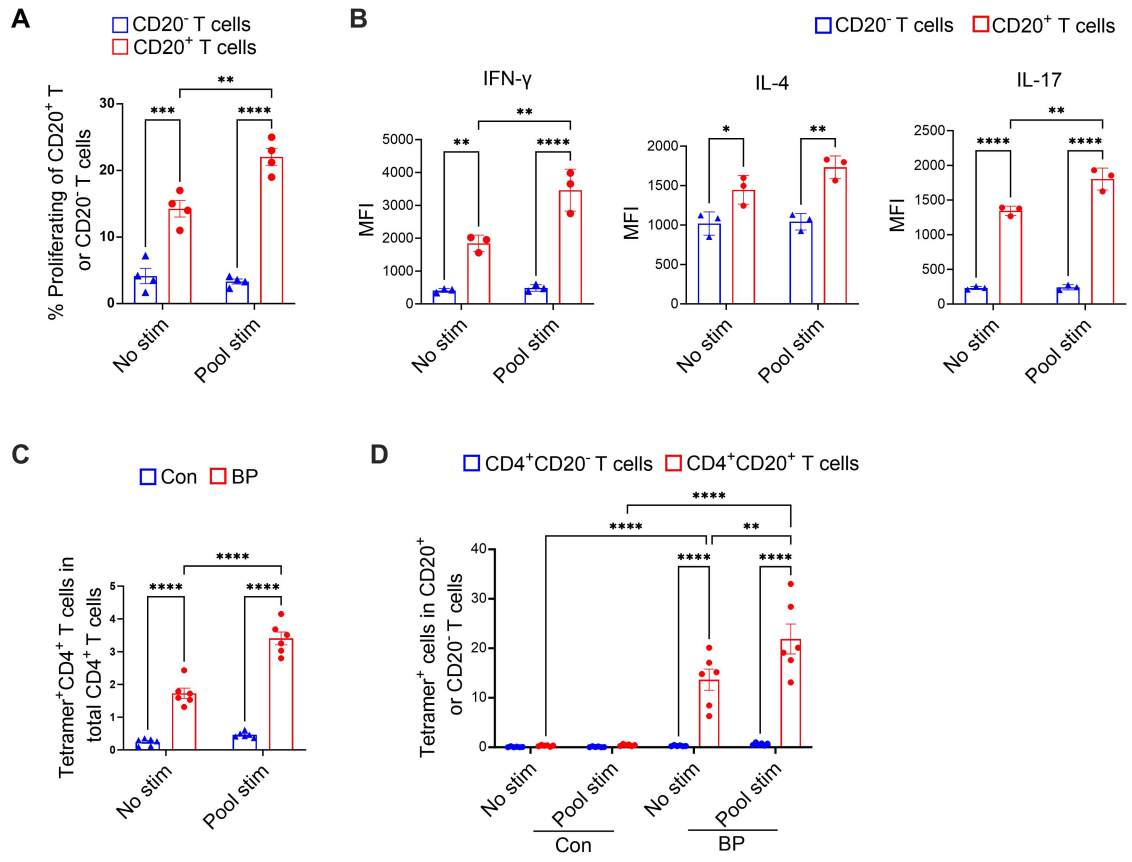

Figure 3. CD20$^+$ T cells exhibit antigen-specific responses in BP patients. (**A**) Percentages of proliferating CD20$^+$ and CD20$^-$ T cells from BP patients with or without peptide stimulation (n = 4). (**B**) Mean fluorescence intensity (MFI) of IFN-γ, IL-4 and IL-17 expression in CD20$^+$ and CD20$^-$ T cells from BP patients under unstimulated or peptide-unstimulated conditions (n = 3). (**C**) Frequencies of tetramer-positive CD4$^+$ T cells in PBMCs collected from untreated BP patients (n = 6) and HLA allele-matched healthy controls (n = 6). (**D**) Frequencies of tetramer-positive T cells within gated CD4$^+$CD20$^+$ and CD4$^+$CD20$^-$ T cell subsets from PBMCs of untreated BP patients (n = 6) and HLA allele-matched healthy controls (n = 6), with or without peptide stimulation. All data are presented as the mean ± SD. Two-way ANOVA with Tukey's post hoc test was used for A, B, C and D. *$P < 0.05$, **$P < 0.01$, ***$P < 0.001$, ****$P < 0.0001$.

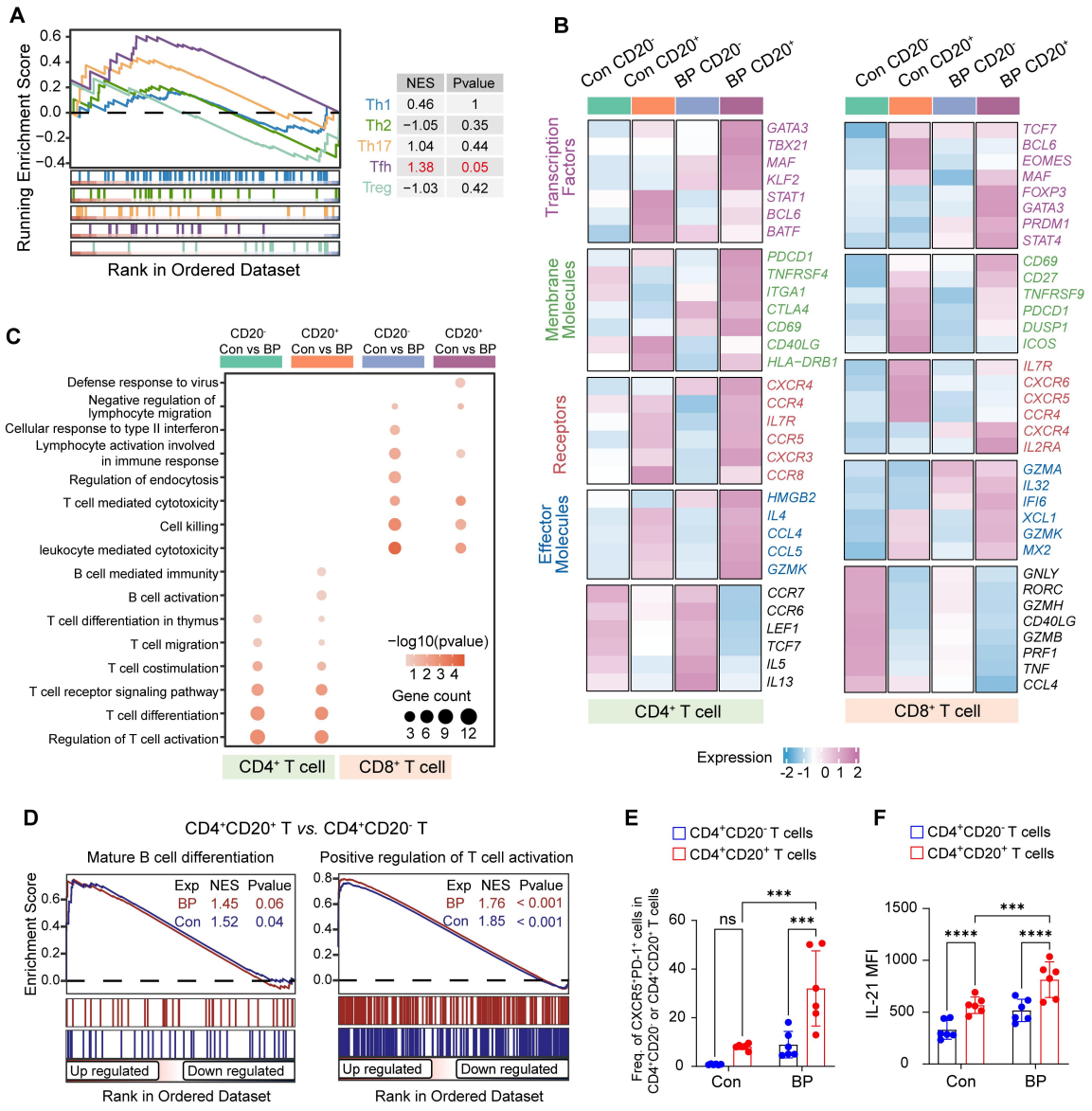

Figure 4. CD4⁺CD20⁺ T cells exhibit Tfh-like characteristics in BP. (**A**) Gene set enrichment analysis (GSEA) enrichment plots for hallmark T cell subsets, comparing CD3⁺CD20⁺ T cells to CD3⁺CD20⁻ T cells in BP patients. (**B**) Single-cell RNA sequencing analysis of CD4⁺CD20⁺ and CD8⁺CD20⁺ T cells from BP patients and healthy controls (Con). Heatmap showing differentially expressed genes (DEGs) comparing CD4⁺CD20⁺ versus CD4⁺CD20⁻ T cells, and CD8⁺CD20⁺ versus CD8⁺CD20⁻ T cells, between Con and BP patients. (**C**) GO analysis of DEGs enriched in the indicated T cell subsets between Con and BP patients. (**D**) GSEA showing enrichment of genes related to mature B cell differentiation and positive regulation of T cell activation in CD4⁺CD20⁺ T cells. (**E**) Frequencies of CXCR5⁺PD-1⁺ T cells within CD4⁺CD20⁺ and CD4⁺CD20⁻ T cells in Con and BP patients (n = 6). (**F**) Mean fluorescence intensity (MFI) of IL-21 expression in CD4⁺CD20⁺ versus CD4⁺CD20⁻ T cells from Con and BP patients (n = 6). All data are presented as the mean ± SD. Two-way ANOVA with Tukey's post hoc test was used for E and F. ****P* < *0.001*, *****P* < *0.0001*.

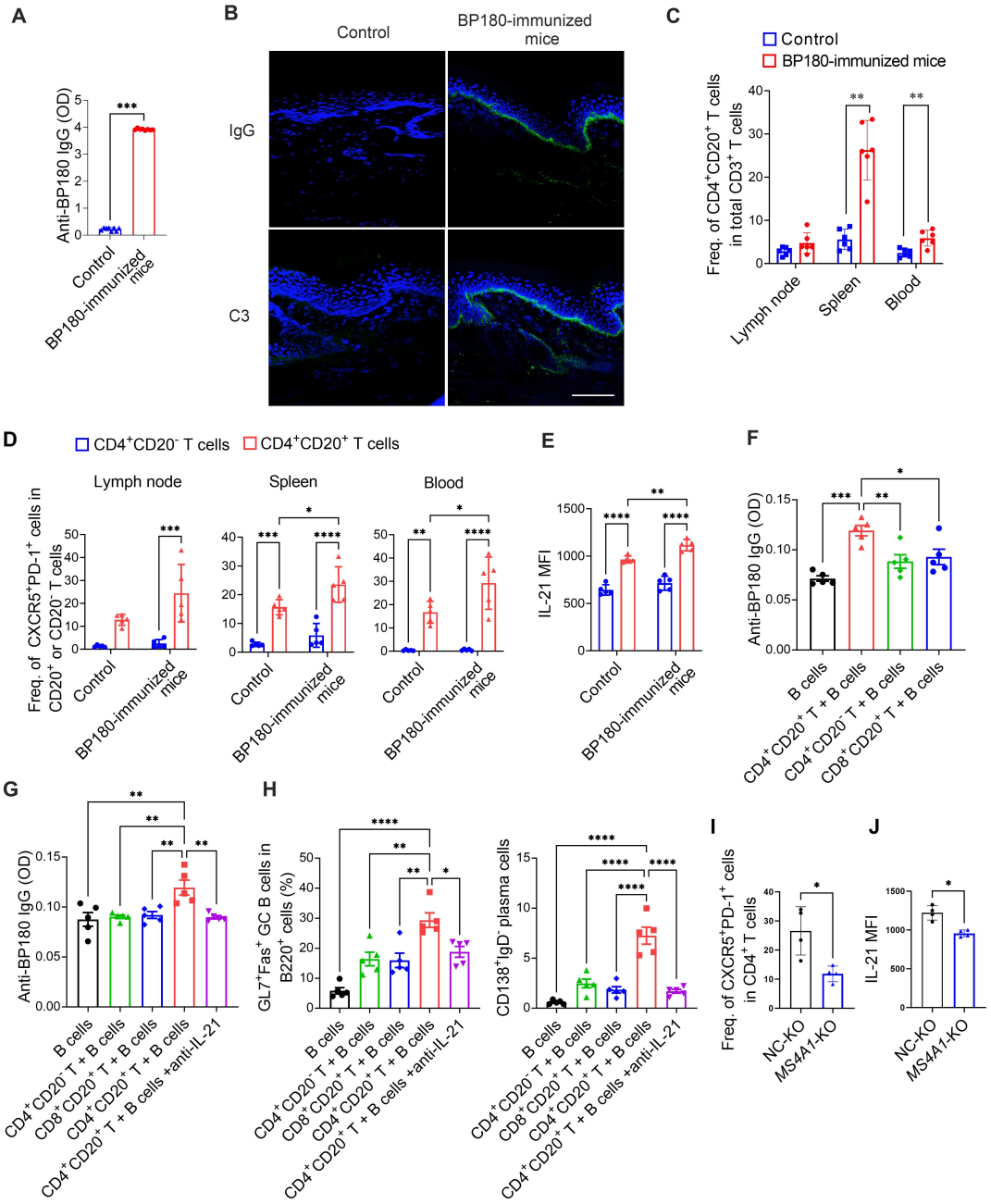

Figure 5. CD20⁺ T cells are increased in BP180-immunized mice and promote B-cell differentiation and antibody production. (**A**) Serum anti-BP180 antibody titers in control and BP180-immunized mice at week 4, as measured by ELISA (n = 8). (**B**) Representative direct immunofluorescence images showing IgG and C3 deposition (green) in back skin sections. Scale bar = 100 μm. (**C**) Frequencies of $CD4^+CD20^+$ T cells in the spleen, lymph nodes, and peripheral blood of control and BP180-immunized mice (n = 6). (**D**) Frequencies of $CXCR5^+PD\text{-}1^+$ cells among $CD4^+CD20^+$ and $CD4^+CD20^-$ T cells in the spleen, lymph nodes and peripheral blood of control and BP180-immunized mice (n = 5). (**E**) Mean fluorescence intensity (MFI) of IL-21 in $CD4^+CD20^+$ or $CD4^+CD20^-$ T cells in the spleen of control and BP180-immunized mice (n = 5).

(**F**) Anti-BP180 antibody titers in cell culture supernatants from each group were measured by ELISA (n = 5). (**G**) Serum anti-BP180 antibody titers in each group of $Rag1^{-/-}$ mice that received adoptive transfer of B cells along with T cell subsets (or B cells alone as control), measured by ELISA (n = 5). (**H**) Frequencies of $GL7^{+}Fas^{+}$ germinal center B cells among $B220^{+}$ B cells and $IgD^{-}CD138^{+}$ plasma cells in $Rag1^{-/-}$ recipient mice (n = 5). (**I**) Frequencies of $CXCR5^{+}PD\text{-}1^{+}$ T cells within $CD4^{+}$ T cells from negative control (NC-KO) and *MS4A1*-knockout (*MS4A1*-KO) T cells (n = 4). (**J**) Mean fluorescence intensity (MFI) of IL-21 in $CD4^{+}$ T cells from control and *MS4A1*-KO T cells (n = 4). All data are presented as the mean ± SD. An unpaired 2-tailed Student's *t* test was used for A, C, I and J; One-way ANOVA with Tukey's post hoc test was used for F, G and H; and two-way ANOVA with Tukey's post hoc test was used for D and E. $*P < 0.05$, $**P < 0.01$, $***P < 0.001$, $****P < 0.0001$.

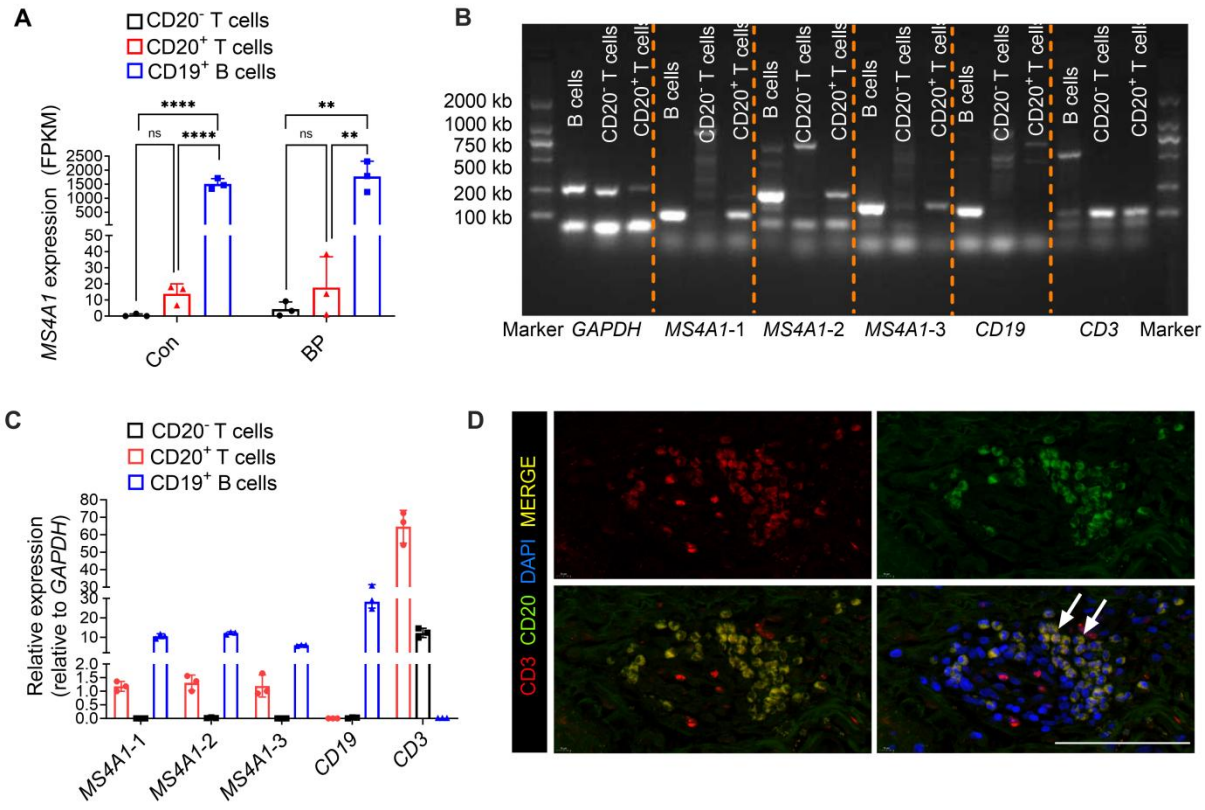

Figure 6. CD20⁺ T cells exhibit endogenous expression of CD20 in human T cells. (**A**) RNA sequencing of CD19⁺ B cells, CD3⁺CD20⁻ T cells, and CD3⁺CD20⁺ T cells obtained via fluorescence-activated cell sorting to evaluate the CD20-encoding gene *MS4A1* (n = 3). (**B**) Agarose gel electrophoresis of qPCR products for *MS4A1*, *CD3*, and *CD19* using cDNA from sorted CD19⁺ B cells, CD3⁺CD20⁻ T cells, and CD3⁺CD20⁺ T cells. (**C**) qPCR analysis of *MS4A1*, *CD3*, and *CD19* expression in sorted CD19⁺ B cells, CD3⁺CD20⁻ T cells, and CD3⁺CD20⁺ T cells from healthy donor peripheral blood, using three independent primer pairs for *MS4A1* (*MS4A1*-1, *MS4A1*-2, *MS4A1*-3) (n = 3). (**D**) Representative RNA in situ hybridization images showing CD3 and CD20 expression in the skin tissue sections of BP patients (n = 2). Scale bar = 100 μm. All data are presented as the mean ± SD. One-way ANOVA with Tukey's post hoc test was used for A. $^{**}P < 0.01$, $^{****}P < 0.0001$.

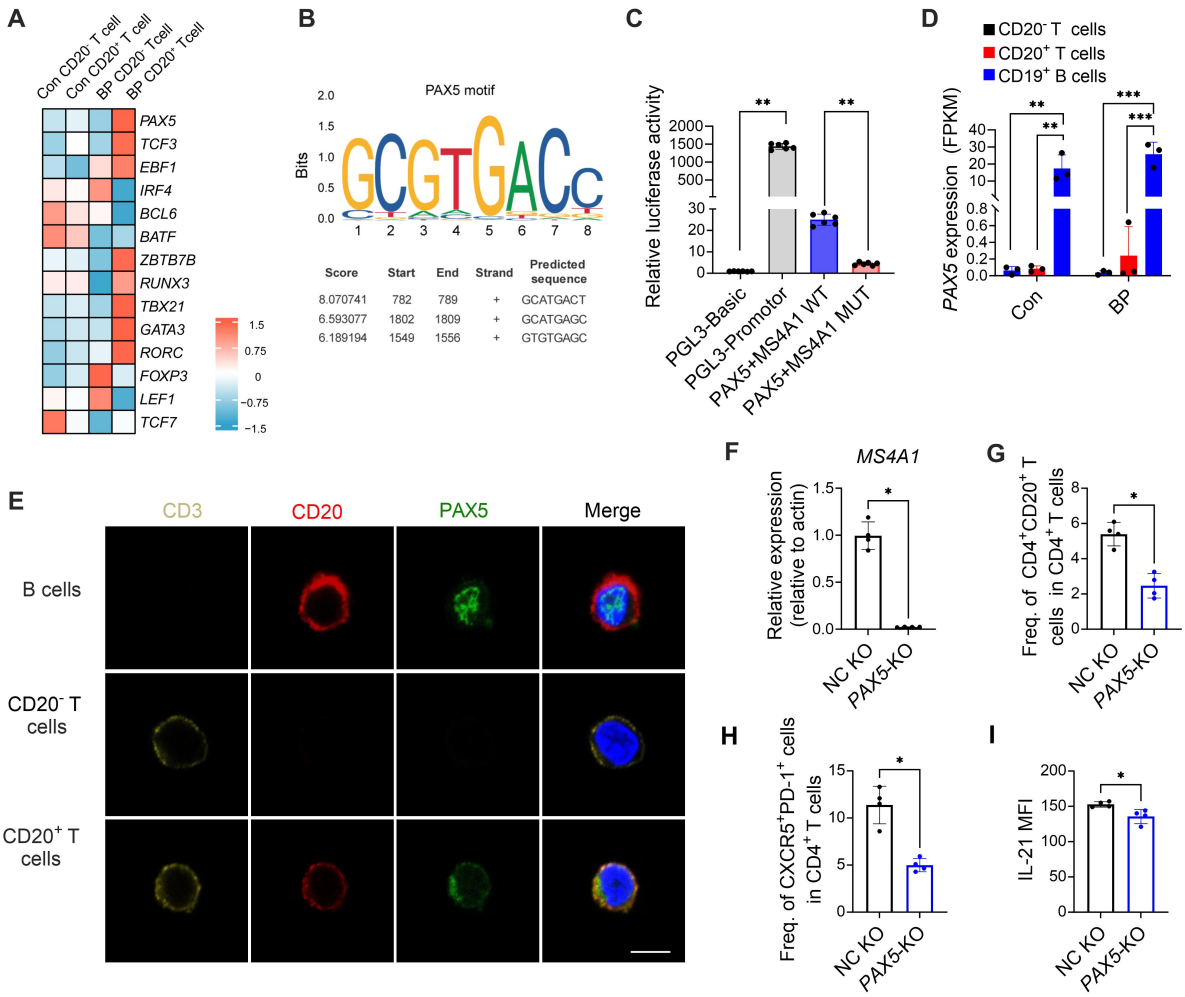

Figure 7. The transcription factor PAX5 regulates endogenous CD20 expression in human CD20⁺ T cells. (**A**) Heatmap showing the top differentially expressed transcription factors between $CD3^+CD20^-$ T cells and $CD3^+CD20^+$ T cells. (**B**) Motifs resembling PAX5-binding motifs within the *MS4A1* regulatory region. (**C**) Luciferase activities of wild-type *MS4A1* and *MS4A1* with a *PAX5*-binding site mutation were determined via luciferase reporter assays in HEK293T cells (n = 6). (**D**) Bulk RNA sequencing analysis of *PAX5* expression *in* FACS-sorted $CD19^+$ B cells, $CD3^+CD20^-$ T cells, and $CD3^+CD20^+$ T cells from Con and BP patients (n = 3). (**E**) Representative immunofluorescence images showing PAX5 (green), CD3 (red), and CD20 (yellow) in sorted human $CD3^+CD20^+$ T cells, $CD3^+CD20^-$ T cells and $CD19^+$ B cells (n = 3). Scale Bar = 5 μm. (**F**) *PAX5* mRNA expression in negative control (NC-KO) or *PAX5*-knockout (*PAX5*-KO) T cells following activated with anti-CD3/CD28 Dynabeads (n = 4). (**G**) Frequencies of $CD4^+CD20^+$ T cells among control or *PAX5*-KO T cells (n = 4). (**H**) Frequencies of $CXCR5^+PD\text{-}1^+$ T cells within $CD4^+$ T cells among control or *PAX5*-KO T cells (n = 4). (**I**) Mean fluorescence intensity (MFI) of IL-21 in $CD4^+$ T cells among control or *PAX5*-KO T cells (n = 4). All data are presented as the mean ± SD. One-way ANOVA with Tukey's post hoc test was used for D. An unpaired 2-tailed Student's *t* test was used for C, F, G, H and I. $*P < 0.05$, $**P < 0.01$, $****P < 0.0001$.

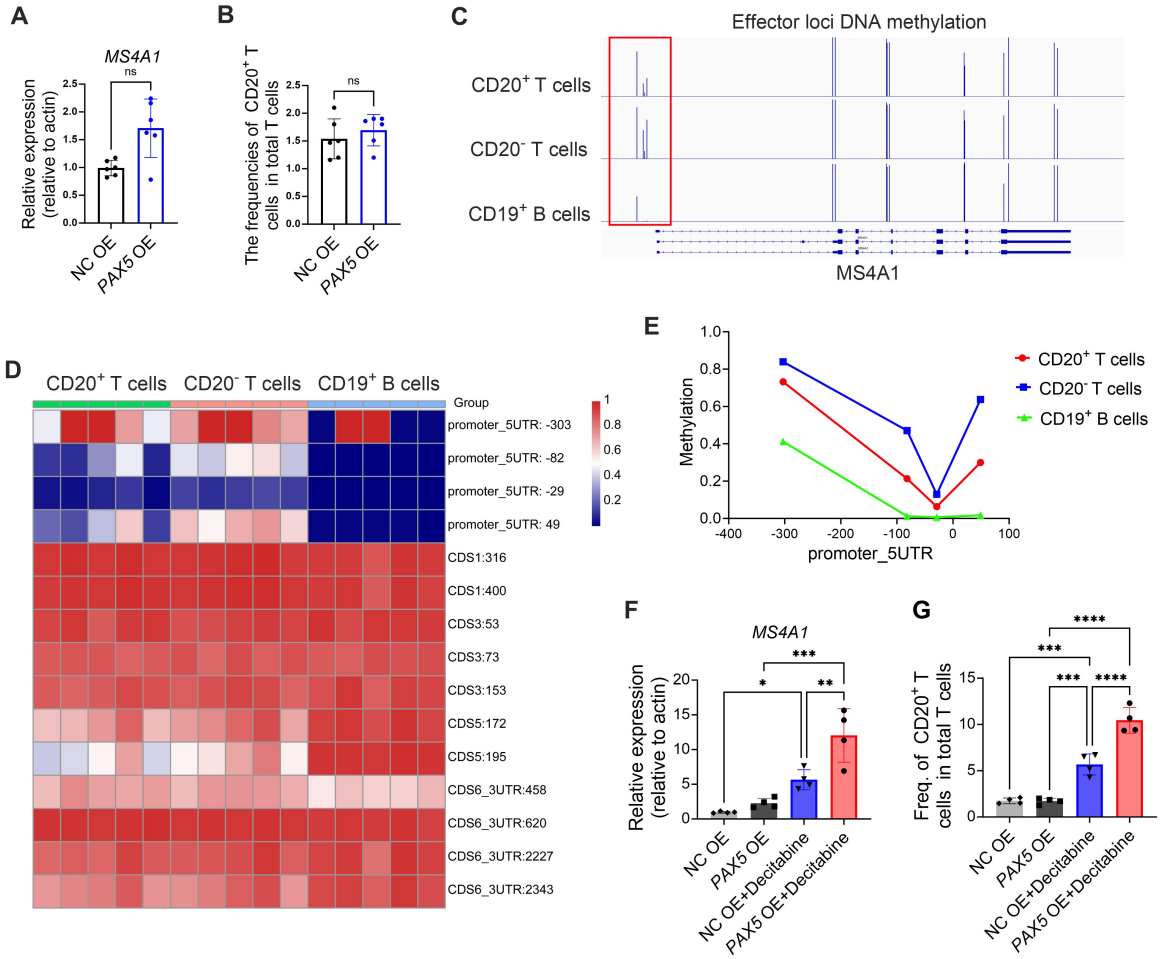

Figure 8. CD20⁺ T cell differentiation is epigenetically regulated by DNA methylation. (**A**) *MS4A1* mRNA expression in negative control (NC) and *PAX5*-overexpressing T cells (*PAX5* OE) following activated with anti-CD3/CD28 Dynabeads (n = 6). (**B**) Frequencies of CD20⁺ T cells in control and *PAX5* OE T cells (n = 6). (**C**) CD3⁺CD20⁺ T cells, CD3⁺CD20⁻ T cells and B cells were sorted from 5 healthy controls (n = 5). Genome browser snapshots of the DNA methylation levels of *MS4A1* across gene regions in these cells. (**D**) Heatmap of the CpG methylation status (promoter and exons) at the *MS4A1* locus in the same cell populations as in (**C**) (n = 5). (**E**) DNA methylation levels at individual CpG sites within the *MS4A1* promoter (positions -303, -82, -29, and +49 relative to the transcription start site) in CD3⁺CD20⁺ T cells, CD3⁺CD20⁻ T cells, and B cells. (**F**) *MS4A1* mRNA expression in control and *PAX5* OE T cells treated with or without decitabine (n = 4). (**G**) Relative frequencies of CD20⁺ T cells among control and *PAX5* OE T cells treated with or without decitabine (n = 4). All data are presented as the mean ± SD. An unpaired 2-tailed Student's *t* test was used for A and B; One-way ANOVA with Tukey's post hoc test was used for F and G. *$P < 0.05$, **$P < 0.01$, ***$P < 0.001$, ****$P < 0.0001$.